A CURRICULUM PERSPECTIVE TO ROBUST LOSS FUNCTIONS

Anonymous authors
Paper under double-blind review

ABSTRACT

Learning with noisy labels is a fundamental problem in machine learning. Much work has been done in designing loss functions that are theoretically robust against label noise. However, it remains unclear why robust loss functions can underfit and why loss functions deviating from theoretical robustness conditions can appear robust. To elucidate these questions, we show that most robust loss functions differ only in the sample-weighting curriculums they implicitly define. The curriculum perspective enables straightforward analysis of the training dynamics with each loss function, which has not been considered in existing theoretical approaches. We show that underfitting can be attributed to marginal sample weights during training, and noise robustness can be attributed to larger weights for clean samples than noisy samples. With a simple fix to the curriculums, robust loss functions that severely underfit can become competitive with the state-of-the-art.[1]

1 INTRODUCTION

Labeling errors are non-negligible from automatic annotation (Liu et al., 2021; Khayrallah & Koehn, 2018), crowd-sourcing (Russakovsky et al., 2015) and expert annotation (Kato & Matsubara, 2010; Bridge et al., 2016). The resulting noisy labels may hamper generalization since over-parameterized neural networks can memorize the training set (Zhang et al., 2017). To combat the adverse impact of noisy labels in classification tasks, a large body of research (Song et al., 2020) aims to design loss functions robust against label noise. Most existing approaches derive sufficient conditions (Ghosh et al., 2017; Zhou et al., 2021b) for noise robustness. Despite the theoretical appeal being agnostic to models and training dynamics[2], they may fail to comprehensively characterize the performance of robust loss functions. Specifically, it has been shown that (1) robust loss functions can underfit difficult tasks (Zhang & Sabuncu, 2018; Wang et al., 2019c; Ma et al., 2020), while (2) loss functions violating existing robustness conditions (Zhang & Sabuncu, 2018; Wang et al., 2019c;b) can exhibit robustness. For (1), existing explanations (Ma et al., 2020; Wang et al., 2019a) can be limited as discussed in §2.2. For (2), to our knowledge, there has been no work directly addressing it.

We analyze training dynamics with various loss functions to elucidate the above observations, which complements existing theoretical approaches. Specifically, we rewrite a broad array of loss functions into a standard form with the same implicit loss function and varied sample-weighting functions (§3), each implicitly defining a sample-weighting curriculum. The interaction between the sample-weighting function and the distribution of implicit losses of samples thus reveals aspects of the training dynamics with each loss function. Here a curriculum by definition (Wang et al., 2020) specifies a sequence of re-weighting for the distribution of training samples, e.g., sample weighting (Chang et al., 2017) or sample selection (Zhou et al., 2021a), based on a metric for sample difficulty. Notably, our novel curriculum perspective first connects robust loss functions to the seemingly distinct curriculum learning approaches (Song et al., 2020) for noise-robust training.

With our curriculum perspective, we first attribute the underfitting issue of robust loss functions to marginal sample weights during training (§4.1). In particular, for classification tasks with numerous classes, the initial sample weights under the curriculum of some robust loss functions can become marginal. When modifying the curriculums accordingly, robust loss functions that severely underfit can become competitive with the state-of-the-art. We then attribute noise robustness of loss functions to larger sample weights for clean samples than for noisy ones during training (§4.2). By examining

[1] Our code will be available at `github`.

[2] Changes of model states during training except for trivial metrics like evaluation metrics and loss functions.

the changes of implicit losses during training, we find that dynamics of SGD suppress the learning of noisy samples. Curriculums of robust loss functions further suppress the learning of noisy samples by magnifying the difference in learning pace between clean and noisy samples while neglecting unlearned noisy samples. Based on our analysis, we present two unexpected phenomenons when viewed from existing theoretical results. By simply changing the learning rate schedule, (1) robust loss functions *can* become vulnerable to label noise, while (2) cross entropy *can* appear robust.

2 BACKGROUND

Classification k-ary classification with input $\boldsymbol{x} \in \mathbb{R}^d$ can be solved by classifier $\arg\max_i s_i$, where s_i is the score for the i-th class in the class scoring function $\boldsymbol{s} : \mathbb{R}^d \to \mathbb{R}^k$ parameterized by $\boldsymbol{\theta}$. Class scores $\boldsymbol{s}(\boldsymbol{x};\boldsymbol{\theta})$ can be turned into class probabilities with the softmax function $p_i = e^{s_i}/(\sum_{j=1}^k e^{s_j})$, where p_i is the probability of class i. Given a loss function $L(\boldsymbol{s}(\boldsymbol{x};\boldsymbol{\theta}), y)$ and data $(\boldsymbol{x}, y)$ with $y \in \{1..k\}$ the ground truth label, $\boldsymbol{\theta}$ can be estimated by risk minimization $\arg\min_{\boldsymbol{\theta}} \mathbb{E}_{\boldsymbol{x},y} L(\boldsymbol{s}(\boldsymbol{x};\boldsymbol{\theta}), y)$, whose solutions are called risk minimizers. We use $\boldsymbol{s}$ in place of $\boldsymbol{s}(\boldsymbol{x};\boldsymbol{\theta})$ for notation simplicity.

Noise robustness Mistakes in the labeling process can corrupt the clean label y into a noisy label

$$\tilde{y} = \begin{cases} y, & \text{with probability } P(\tilde{y} = y|\boldsymbol{x}, y) \\ i,\ i \neq y & \text{with probability } P(\tilde{y} = i|\boldsymbol{x}, y) \end{cases}$$

Label noise is symmetric (or uniform) if $P(\tilde{y} = i|\boldsymbol{x}, y) = \eta/(k-1), \forall i \neq y$, with $\eta = P(\tilde{y} \neq y)$ the noise rate constant. Label noise is asymmetric (or class-conditional) if $P(\tilde{y} = i|\boldsymbol{x}, y) = P(\tilde{y} = i|y)$. Given data $(\boldsymbol{x}, \tilde{y})$ with noisy label $\tilde{y}$, a loss function L is robust against label noise if

$$\arg\min_{\boldsymbol{\theta}} \mathbb{E}_{\boldsymbol{x},\tilde{y}} L(\boldsymbol{s}(\boldsymbol{x};\boldsymbol{\theta}), \tilde{y}) = \arg\min_{\boldsymbol{\theta}} \mathbb{E}_{\boldsymbol{x},y} L(\boldsymbol{s}(\boldsymbol{x};\boldsymbol{\theta}), y) \tag{1}$$

Conditions for noise robustness Most existing approaches on robust loss function (Ghosh et al., 2017; Ma et al., 2020; Liu & Guo, 2020; Feng et al., 2020; Zhou et al., 2021b) focus on bounding the difference between risk minimizers obtained with noisy and clean data, i.e., ensuring that Eq. (1) approximately holds. These bounds only depend on the loss functions and mild assumptions about the dataset. To contrast our curriculum perspective with these approaches, we review two typical sufficient conditions for noise robustness. Loss function L is symmetric (Ghosh et al., 2017) if

$$\sum\nolimits_{i=1}^k L(\boldsymbol{s}, i) = C,\ \forall \boldsymbol{s} \in \mathbb{R}^k, \tag{2}$$

where C is a constant. It is robust against *symmetric* label noise with $\eta < (k-1)/k$. This stringent condition was later relaxed to the asymmetric condition. To rephrase, a loss function as a function of the softmax probability p_i, i.e., $L(\boldsymbol{s}, i) = l(p_i)$, is asymmetric (Zhou et al., 2021b) if

$$\max_{i \neq y} \frac{P(\tilde{y} = i|\boldsymbol{x}, y)}{P(\tilde{y} = y|\boldsymbol{x}, y)} = \tilde{r} \leq r = \inf_{\substack{0 \leq p_i, \Delta p \leq 1 \\ p_i + \Delta p \leq 1}} \frac{l(p_i) - l(p_i + \Delta p)}{l(0) - l(\Delta p)}, \tag{3}$$

where Δp is a valid increment of p_i. When clean labels dominate the data, i.e., $\tilde{r} < 1$, an asymmetric loss is robust against *generic* label noise.

The active-passive dichotomy Ma et al. (2020) draw a distinction between active and passive loss functions. By rewriting loss function L into a sum of basic functions, $L(\boldsymbol{s}, y) = \sum_{i=1}^k l(\boldsymbol{s}, i)$, active loss functions can be defined with $\forall i \neq y,\ l(\boldsymbol{s}, i) = 0$, which emphasizes learning the target label. In contrast, passive loss functions defined with $\exists i \neq y,\ l(\boldsymbol{s}, i) \neq 0$ can be improved by unlearning the non-target labels. However, since there is no canonical guideline to specify $l(\boldsymbol{s}, i)$, different specifications can lead to ambiguities in the active-passive dichotomy as discussed in §2.2.

In summary, the above research fails to address open questions in §2.2. Since many loss functions degrade less in performance than cross entropy under label noise, exhibiting various degrees of noise robustness, as a slight abuse of terminology, we refer to them as robust loss functions hereafter.

2.1 TYPICAL ROBUST LOSS FUNCTIONS

In addition to cross entropy (CE) that is vulnerable to label noise (Ghosh et al., 2017), we review typical robust loss functions for later analysis. We ignore differences in constant scaling factors and additive biases, as they are either equivalent to learning rate scaling in SGD or irrelevant in the

gradient computation. See Table 1 for the formulas and Appendix A for a comprehensive review of additional loss functions.

Symmetric The mean absolute error (MAE; Ghosh et al., 2017) and the equivalent reverse cross entropy (RCE; Wang et al., 2019c) are both symmetric as they satisfy Eq. (2). Ma et al. (2020) make loss functions satisfying $L(\boldsymbol{s}, i) > 0, \forall i \in \{1..k\}$ symmetric by normalizing them with $L_{\mathrm{N}}(\boldsymbol{s}, y) = L(\boldsymbol{s}, y)/(\sum_{i=1}^{k} L(\boldsymbol{s}, i))$. We include normalized cross entropy (NCE; Ma et al. 2020) as an example.

Asymmetric We include asymmetric generalized cross entropy (AGCE) and asymmetric unhinged loss (AUL) proposed by Zhou et al. (2021b) as typical asymmetric loss functions. Notably, AGCE with $q \geq 1$ and AUL with $q \leq 1$ are completely asymmetric, i.e., Eq. (3) always holds when $\tilde{r} < 1$.

Combined Loss functions can be combined for both robustness and sufficient learning. For example, generalized cross entropy (GCE; Zhang & Sabuncu, 2018) is a smooth interpolation between CE and MAE. Alternatively, symmetric cross entropy (SCE; Wang et al., 2019c) is a weighted average of CE and RCE (MAE). Ma et al. (2020) argue that robust and sufficient training requires a balanced combination of active and passive loss functions. Accordingly to their active-passive dichotomy, CE and NCE are active while MAE (RCE) is passive. We include NCE+MAE as an example.

2.2 Open Questions

Why do robust loss functions underfit? Ma et al. (2020) attribute underfitting to failure in balancing active-passive components. However, the active-passive dichotomy can be ambiguous. Given

$$L_{\mathrm{MAE}}(\boldsymbol{s}, y) \propto \sum\nolimits_{i=1}^{k} |\mathbb{I}(i = y) - p_i| \propto \sum\nolimits_{i=1}^{k} \mathbb{I}(i = y)(1 - p_i)$$

where $\mathbb{I}(\cdot)$ is the indicator function, MAE is passive with $l(\boldsymbol{s}, i) = |\mathbb{I}(i = y) - p_i|$ but active with $l(\boldsymbol{s}, i) = \mathbb{I}(i = y)(1 - p_i)$. Wang et al. (2019a) view $\|\nabla_{\boldsymbol{s}} L(\boldsymbol{s}, y)\|_1$ as weights for sample gradients and attribute underfitting to their low variance, making clean and noisy samples less distinguishable. However, as we show in §4.1, MAE also underfits data with clean labels. In summary, neither Ma et al. (2020) nor Wang et al. (2019a) fully explain the underfitting issue.

What affects the robustness of a loss function? Although combined loss functions such as GCE and SCE fail to satisfy Eq. (2) and (3), it is unclear why they exhibit robustness against label noise (Zhang & Sabuncu, 2018; Wang et al., 2019c). Furthermore, it is unclear how training dynamics with loss functions, which are irrelevant in theoretical robustness guarantees (Ghosh et al., 2017; Zhou et al., 2021b; Ma et al., 2020; Liu & Guo, 2020; Feng et al., 2020), affect their noise robustness.

3 Implicit Curriculums of Loss Functions

Loss functions in Table 1 except NCE can be written as a function of the target softmax probability p_y, i.e., $L(\boldsymbol{s}, y) = l(p_y)$. A close examination of p_y gives

$$p_y = \frac{e^{s_y}}{\sum_{i=1}^{k} e^{s_i}} = \frac{1}{e^{\log \sum_{i \neq y} e^{s_i - s_y}} + 1} = \frac{1}{e^{-\Delta_y} + 1} = \mathrm{sigmoid}(\Delta_y), \tag{4}$$

where

$$\Delta_y = s_y - \log \sum\nolimits_{i \neq y} e^{s_i} \leq s_y - \max\nolimits_{i \neq y} s_i \tag{5}$$

indicates how well a sample is learned, as $\Delta_y \geq 0$ ensures successful classification $y = \arg\max_i s_i$. Loss functions with the form $L(\boldsymbol{s}, y) = l(p_y)$ can thus be rewritten into a standard form with *equivalent gradients*, i.e.,

$$L(\boldsymbol{s}, y) = l(p_y) = \int_{\boldsymbol{s}} \nabla_{\boldsymbol{s}} l(p_y) \mathrm{d}\boldsymbol{s} = \int_{\boldsymbol{s}} l'(p_y) p_y'(\Delta_y) \cdot \nabla_{\boldsymbol{s}} \Delta_y \mathrm{d}\boldsymbol{s} = -w(\Delta_y) \cdot \Delta_y, \tag{6}$$

where $w(\Delta_y) = |l'(p_y) p_y'(\Delta_y)|$ is a scalar weight wrapped with the stop-gradient operator, and Δ_y is an implicit loss function embedded in $L(\boldsymbol{s}, y)$. Loss functions following Eq. (6) thus implicitly define different sample-weighting curriculums, with $w(\Delta_y)$ the sample-weighting function and Δ_y the metric for sample difficulty. Notably, Δ_y factors out the preference from $w(\Delta_y)$, making it a more direct metric for sample difficulty than those based on losses (Kumar et al., 2010) or gradient magnitudes (Gopal, 2016). In addition, the interaction between $w(\Delta_y)$ and Δ_y distributions reveals aspects of the training dynamics with each loss function. See Table 1 for a summary of $w(\Delta_y)$ for the reviewed loss functions, and Appendix A for how hyperparameters affect $w(\Delta_y)$.

Type	Name	Function	Sample Weight w	Constraints
/	CE	$-\log p_y$	$1-p_y$	/
Sym.	MAE/RCE	$1-p_y$	$p_y(1-p_y)$	/
	NCE	$-\log p_y / \left(\sum_{i=1}^{k} -\log p_i\right)$	/	/
Asym.	AUL	$[(a-p_y)^q-(a-1)^q]/q$	$p_y(1-p_y)(a-p_y)^{q-1}$	$a>1, q>0$
	AGCE	$[(a+1)-(a+p_y)^q]/q$	$p_y(a+p_y)^{q-1}(1-p_y)$	$a>0, q>0$
Comb.	GCE	$(1-p_y^q)/q$	$p_y^q(1-p_y)$	$0<q\leq 1$
	SCE	$(1-q)\cdot L_{\mathrm{CE}}+q\cdot L_{\mathrm{MAE}}$	$(1-q+q\cdot p_y)(1-p_y)$	$0<q<1$
	NCE+MAE	$(1-q)\cdot L_{\mathrm{NCE}}+q\cdot L_{\mathrm{MAE}}$	/	$0<q<1$

Table 1: Expressions, constraints and sample-weighting functions (§3) for loss functions in §2.1.

3.1 The Additional Regularizer of NCE

NCE does not follow Eq. (6) as it additionally depends on $p_i, i \neq y$. Yet it can be rewritten into

$$L_{\mathrm{NCE}}(\boldsymbol{s}, y) = \gamma_{\mathrm{NCE}} \cdot L_{\mathrm{CE}}(\boldsymbol{s}, y) + \gamma_{\mathrm{NCE}} \cdot \epsilon_{\mathrm{NCE}} \cdot R_{\mathrm{NCE}}(\boldsymbol{s}), \tag{7}$$

where $\gamma_{\mathrm{NCE}} = 1/(\sum_{i=1}^{k} -\log p_i)$ and $\epsilon_{\mathrm{NCE}} = k(-\log p_y)/(\sum_{i=1}^{k} -\log p_i)$ are scalar weights wrapped with the stop-gradient operator. In Eq. (7), the first term is a *primary loss function* defining a sample-weighting curriculum similar to CE. The second is a *regularizer*

$$R_{\mathrm{NCE}}(\boldsymbol{s}) = \sum\nolimits_{i=1}^{k} \frac{1}{k} \log p_i$$

reducing the entropy of the softmax output. Although the training dynamics of NCE are complicated by $R_{\mathrm{NCE}}(\boldsymbol{s})$, we can use the upperbound for the L1 norm of gradient $\nabla_{\boldsymbol{s}} L_{\mathrm{NCE}}(\boldsymbol{s}, y)$,

$$\hat{w}_{\mathrm{NCE}} = 2\gamma_{\mathrm{NCE}} \cdot w_{\mathrm{CE}} \left(1 + \epsilon_{\mathrm{NCE}}\right) \geq \|\nabla_{\boldsymbol{s}} L_{\mathrm{NCE}}(\boldsymbol{s}, y)\|_1, \tag{8}$$

as the weight of each sample in gradient updates. Examining how $\hat{w}_{\mathrm{NCE}}$ changes during training helps understand why NCE underfits in §4.1. We leave the derivations to Appendix A.5.1 and discussions about similar loss functions to Appendix A.5.

4 Robust Loss Functions from the Curriculum Perspective

We examine the interaction between $w(\Delta_y)$ and Δ_y distributions to address questions in §2.2. Results are reported on MNIST (Lecun et al., 1998) and CIFAR10/100 (Krizhevsky, 2009) with synthetic symmetric and asymmetric label noise following Ma et al. (2020); Zhou et al. (2021b). For real-world scenarios, we include CIFAR10/100 with human label noise (Wei et al., 2022) and the large-scale noisy dataset WebVision (Li et al., 2017), which exhibit more complex noise patterns than symmetric and asymmetric label noise. Unlike standard settings, we scale $w(\Delta_y)$ to unit maximum to avoid complications, since hyperparameters of loss functions can change the scale of $w(\Delta_y)$, essentially adjusting the learning rate of SGD. See Appendix B for more experimental details.

4.1 Understanding Underfitting of Robust Loss Functions

Robust loss functions can underfit We confirm that on difficult tasks like CIFAR100 (Song et al., 2020), underfitting can result from robust loss functions themselves rather than inferior hyperparameters. As shown in Table 2, CE outperforms NCE, AGCE and AUL by a nontrivial margin on CIFAR100. In particular, MAE performs much worse than CE, similar to AGCE† and AUL† with inferior hyperparameters. See Table 9 for similar results with learning rate $\alpha = 0.01$.

Marginal sample weights explains underfitting The effective scale of parameter update at step t during SGD can be approximated by $\alpha_t^* = \alpha_t \cdot \bar{w}_t$, which depends on the average sample weight $\bar{w}_t$ of the batch and the learning rate α_t. We use $\bar{\alpha}_t^* = \sum_{i=1}^{t} \alpha_i^*/t$ to characterize the overall α_t^*

Underfitting	Loss	CIFAR100 Acc.	CIFAR100 $\bar{\alpha}_t^*$	CIFAR10 Acc.	CIFAR10 $\bar{\alpha}_t^*$
/	CE	71.33 ± 0.23	8.183	92.76 ± 0.30	5.541
No	SCE	71.36 ± 0.39	9.541	93.17 ± 0.06	7.018
	GCE	69.95 ± 0.40	8.861	92.96 ± 0.13	6.151
	NCE+MAE	68.89 ± 0.23	/	92.37 ± 0.33	/
Moderate	AUL	58.75 ± 1.07	5.278	92.43 ± 0.19	5.171
	AGCE	49.27 ± 1.03	4.537	92.61 ± 0.18	5.225
	NCE	43.18 ± 1.55	/	91.28 ± 0.22	/
Severe	MAE	3.69 ± 0.59	0.035	91.56 ± 0.11	2.492
	AUL†	3.13 ± 0.43	0.033	91.13 ± 0.06	2.308
	AGCE†	1.62 ± 0.69	0.009	87.14 ± 4.96	1.701

Table 2: Without label noise, robust loss functions can underfit CIFAR100 but CIFAR10. Hyperparameters of loss functions are tuned on CIFAR100 and listed in Table 8. We report test accuracy and $\bar{\alpha}_t^*$ (scaled by 10^3) at the final training step from 3 different runs with learning rate $\alpha = 0.1$. Loss functions with inferior hyperparameters (denoted with †) are included as references. See Table 9 for similar results with learning rate $\alpha = 0.01$.

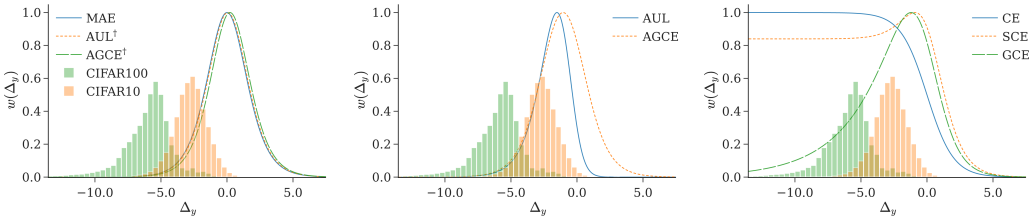

(a) Severe underfitting (b) Moderate underfitting (c) No underfitting

Figure 1: Sample-weighting functions $w(\Delta_y)$ of loss functions in Table 2 with hyperparameters in Table 8. We include the initial Δ_y distributions of CIFAR10 and CIFAR100 for reference, which are obtained by computing Δ_y with a randomly initialized model for all training samples.

up to step t. In Table 2, for loss functions that heavily underfit on CIFAR100, $\bar{\alpha}_t^*$ at the final step is marginal compared to CE, suggesting a marginal overall sample weight during training given the same learning rate schedule.

Underfitting from fast diminishing sample weights Similar to CE, in Fig. 2a, $\bar{\alpha}_t^*$ of NCE based on $\hat{w}_{\text{NCE}}$ peaks at initialization. However, it decreases much faster than CE since both γ_{NCE} and w_{CE} decrease with improved Δ_y. In addition, the regularizer $R_{\text{NCE}}(\boldsymbol{s})$ further reduces the entropy of softmax output and thus γ_{NCE}. The resulting fast decreasing $\hat{w}_{\text{NCE}}$ hampers the learning of training samples, which can lead to underfitting.

Underfitting from marginal initial sample weights In Fig. 1a, unlike NCE, loss functions that severely underfit in Table 2 assign marginal weights to samples in CIFAR100 at initialization, which leads to marginal initial $\bar{\alpha}_t^*$. Δ_y of these samples can barely improve before the learning rate vanishes, thus leading to underfitting. In contrast, loss functions with non-trivial initial sample weights (Fig. 1b and 1c) result in moderate or no underfitting. As further corroboration, we plot $\bar{\alpha}_t^*$ of AUL with superior and inferior hyperparameters (AUL and AUL† in Table 2) in Fig. 2b. $\bar{\alpha}_t^*$ stays marginal with AUL†, but quickly increases to a non-negligible value before gradually decreasing with AUL.

Loss combination can mitigate underfitting. As $\hat{w}_{\text{NCE}}$ peaks at initialization but quickly diminishes while w_{MAE} is marginal at initialization but peaks later during training, combining NCE with MAE can mitigate the underfitting issue of each other. In Table 2, combining NCE and MAE suffers less from underfitting compared to both individuals.

Increased number of classes leads to marginal initial sample weights. Unlike CIFAR100, all loss functions in Table 2 perform equally well on CIFAR10. Such a difference has been vaguely attributed to the increased task difficulty of CIFAR100 (Zhang & Sabuncu, 2018; Song et al., 2020). Intuitively, the more classes, the more subtle differences to be distinguished. In addition, the number of classes k determines the initial distribution of Δ_y. Assume that class scores s_i at *initialization* are i.i.d. normal variables $s_i \sim \mathcal{N}(\mu, \sigma)$. In particular, $\mu = 0$ and $\sigma = 1$ for most neural networks with standard initializations (Glorot & Bengio, 2010; He et al., 2015) and normalization layers (Ioffe &

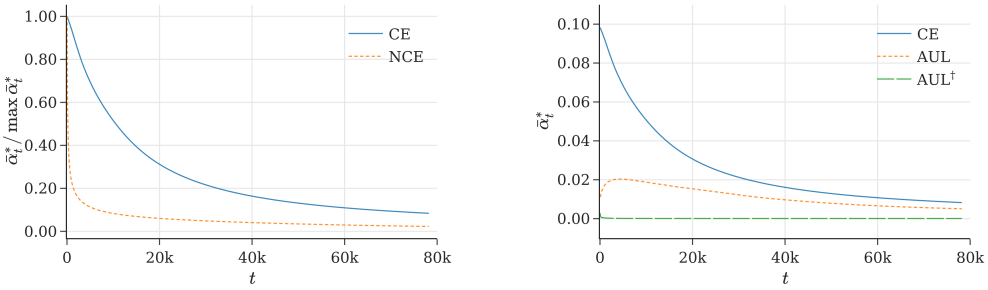

(a) NCE with estimated weight upperbound.

(b) AUL with inferior/superior hyperparameters.

Figure 2: Different explanations for underfitting: (a) fast diminishing sample weights; (b) marginal initial sample weights. We plot the variation of $\bar{\alpha}_t^*$ with training step t on CIFAR100 without label noise for each loss function. $\bar{\alpha}_t^*$ of NCE is estimated with $\hat{w}_{\mathrm{NCE}}$. Since $\hat{w}_{\mathrm{NCE}}$ is not comparable to w_{CE}, we normalize $\bar{\alpha}_t^*$ with its maximum in (a) to emphasize its variation during training.

Loss	Clean $\eta = 0$	Symmetric $\eta = 0.4$	Symmetric $\eta = 0.8$	Asymmetric $\eta = 0.4$	Human $\eta = 0.4$
CE‡	71.33 ± 0.43	39.92 ± 0.10	7.59 ± 0.20	40.17 ± 1.31	/
GCE‡	63.09 ± 1.39	56.11 ± 1.35	17.42 ± 0.06	40.91 ± 0.57	/
NCE‡	29.96 ± 0.73	19.54 ± 0.52	8.55 ± 0.37	20.64 ± 0.40	/
NCE+AUL‡	68.96 ± 0.16	59.25 ± 0.23	23.03 ± 0.64	38.59 ± 0.48	/
AGCE	49.27 ± 1.03	47.76 ± 1.75	16.03 ± 0.59	33.40 ± 1.57	30.45 ± 1.50
AGCE shift	69.39 ± 0.84	48.21 ± 1.06	14.49 ± 0.17	40.76 ± 0.74	48.71 ± 0.45
AGCE scale	70.57 ± 0.62	56.69 ± 0.33	14.64 ± 0.79	39.71 ± 0.17	50.85 ± 0.11
MAE	3.69 ± 0.59	1.29 ± 0.50	1.00 ± 0.00	2.53 ± 1.34	2.09 ± 0.55
MAE shift	68.57 ± 0.54	49.95 ± 0.16	13.10 ± 0.41	39.83 ± 0.18	47.91 ± 0.36
MAE scale	**70.97 ± 0.41**	**60.57 ± 1.04**	**24.44 ± 0.73**	**44.48 ± 1.05**	**54.70 ± 0.48**

Table 3: Shifting or scaling $w(\Delta_y)$ mitigates underfitting on CIFAR100 under different label noise. We report test accuracies with 3 different runs. Results from Zhou et al. (2021b) are included as context (denoted with ‡). See Table 10 for hyperparameter τ of each setting, and Tables 11 and 12 for results with more noise rates.

Szegedy, 2015; Ba et al., 2016). The expected Δ_y can be approximated with

$$\mathbb{E}[\Delta_y] \approx -\log(k-1) - \sigma^2/2 + \frac{e^{\sigma^2} - 1}{2(k-1)} \tag{9}$$

We leave derivations and comparisons between our assumptions and real settings to Appendix C.1. A large k results in small initial Δ_y; with sample-weighting functions in Fig. 1a it further leads to marginal initial sample weights, which results in underfitting on CIFAR100 as discussed previously.

4.1.1 Addressing Underfitting from Marginal Initial Sample Weights

Our analysis suggests that the fixed sample-weighting function $w(\Delta_y)$ is to blame for underfitting. To make the initial sample weights agnostic to the number of classes, we can simply scale

$$w^*(\Delta_y) = w(\Delta_y / |\mathbb{E}[\Delta_y]| \cdot \tau)$$

or shift

$$w^+(\Delta_y) = w(\Delta_y + |\mathbb{E}[\Delta_y]| - \tau)$$

the sample-weighting functions, where τ is a hyperparameter. Intuitively, $|\mathbb{E}[\Delta_y]|$ in $w^*(\Delta_y)$ and $w^+(\Delta_y)$ cancels the effect of k on the weight of the expected initial Δ_y. A small τ thus leads to high initial sample weights regardless of k. See Fig. 7 for a visualization of $w^*_{\mathrm{MAE}}(\Delta_y)$ and $w^+_{\mathrm{MAE}}(\Delta_y)$. Results on CIFAR100 with different label noise are reported in Table 3. See Tables 11 and 12 in Appendix C.1.1 for results with additional noise rates. We also report results on the large-scale WebVision dataset with different numbers of classes in Table 4. In summary, shifting and scaling alleviate underfitting, making MAE and AGCE comparable to the previous state-of-the-art (NCE+AUL; Zhou et al. 2021b). Notably, $w^*(\Delta_y)$ leads to dramatic improvements for MAE under all settings.

Settings	$k = 50$ $\tau = 2.0$	$k = 200$ $\tau = 1.8$	$k = 400$ $\tau = 1.6$
CE	66.40	70.26	70.16
MAE	3.68	0.50	0.25
MAE shift	60.76	59.31	47.32
MAE scale	**66.72**	**71.92**	**71.87**

Table 4: Shifting or scaling $w(\Delta_y)$ mitigates underfitting on WebVision subsampled with different numbers of classes. $k = 50$ is the standard "mini" setting in previous work (Ma et al., 2020; Zhou et al., 2021b). We report test accuracy with a single run due to a limited computation budget.

	Clean	Asymmetric		Symmetric						Human	
		$\eta = 0.2$		$\eta = 0.2$		$\eta = 0.4$		$\eta = 0.8$		$\eta = 0.4$	
Loss	Acc	diff	snr	diff	snr	diff	snr	diff	snr	diff	snr
CE	90.64	-7.06	0.32	-15.47	0.39	-31.95	0.57	-50.87	0.77	-28.51	0.53
SCE	89.87	-5.39	0.51	-3.84	0.99	-10.47	1.27	-27.25	1.51	-15.84	0.86
GCE	90.44	-7.42	0.36	-6.80	0.96	-23.23	0.89	-45.32	1.04	-21.94	0.72
AUL	89.90	-2.51	0.81	-2.07	3.10	-5.87	2.96	-13.90	2.83	-12.08	1.11
MAE	89.29	-2.21	1.00	-1.92	3.56	-4.36	3.33	-11.53	3.22	-10.35	1.32
AGCE	82.62	-9.42	0.92	-1.55	3.02	-19.90	2.16	-41.11	1.83	-21.73	1.28

Table 5: Robust loss functions assign larger weights to clean samples. We report snr and diff from the best of 5 runs on CIFAR10 under each noise setting, as inferior initialization can substantially degrade the performance. Hyperparameters are selected to cover more variants of sample-weighting functions, which are not necessarily optimal. See Table 13 for hyperparameters and Fig. 8 for plots of the sample-weighting functions.

Although $w^*(\Delta_y)$ and $w^+(\Delta_y)$ are agnostic to the number of classes at initialization, their performances differ significantly. Intuitively, $w^+(\Delta_y)$ diminishes much faster than $w^*(\Delta_y)$ with increased Δ_y, which can lead to insufficient training of clean samples and thus inferior performance.

4.2 Understanding Noise Robustness of Loss Functions

We show that robust loss functions following Eq. (6) *implicitly* assign larger weights to clean samples. The underlying reasons are explored by examining how Δ_y distributions change during training. Notably, similar sample-weighting rules are *explicitly* adopted by curriculums for noise robust training (Ren et al., 2018). We leave NCE to future work as it involves an additional regularizer.

Robust loss functions assign larger weights to clean samples. We use the ratio between the average weights of clean ($\bar{w}_{\text{clean}}$) and noisy ($\bar{w}_{\text{noise}}$) samples, $\mathrm{snr} = \bar{w}_{\text{clean}}/\bar{w}_{\text{noise}}$, to characterize their relative contribution during training. See Appendix C.2 for the exact formulas. Noise robustness is characterized by differences in test accuracy compared to results with clean labels (diff). We report diff and snr under different label noise on CIFAR10 in Table 5. Loss functions with higher snr have less performance drop with label noise in general, thus being more robust.

To explain what leads to a large snr, we plot changes of Δ_y distributions during training on CIFAR10 with symmetric label noise in Fig. 3. See Fig. 9 and 10 for similar results with additional types of label noise and loss functions. When trained with loss functions that are more robust against label noise (Fig. 3b and 3c), Δ_y distributions of noisy and clean samples spread wider and get better separated. In addition, the consistent decrease of Δ_y for noisy samples suggests that they can be *unlearned*. In contrast, training with CE (Fig. 3a) results in more compact and less separated Δ_y distributions. Furthermore, Δ_y of noisy samples consistently increases.

Dynamics of SGD suppress learning of noisy samples. As shown in Fig. 3a, noisy samples are learned slower than clean samples as measured by improvements of Δ_y, which can be explained by more coherent gradients among clean samples (Chatterjee & Zielinski, 2022). Similar results have been reported (Zhang et al., 2017; Arpit et al., 2017) and utilized in curriculum-based robust training (Yao et al., 2019; Han et al., 2018). In addition, noisy samples can be unlearned as shown in Fig. 3b and 3c, which can stem from generalization with clean samples. Both dynamics suppress the learning of noisy samples but clean ones, thus leading to robustness against label noise.

Robust $w(\Delta_y)$ synergizes with SGD dynamics for noise robustness. In Fig. 1, the bell-shaped $w(\Delta_y)$ of robust loss functions only assigns large weights to samples with moderate Δ_y. Since Δ_y

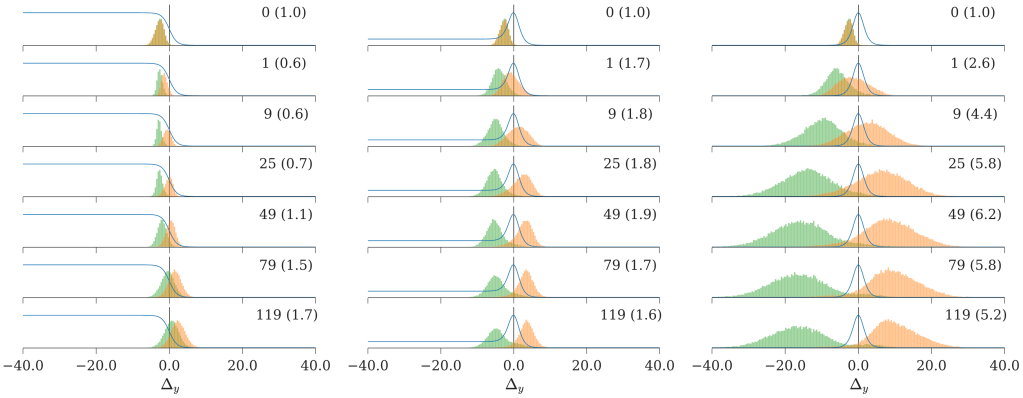

(a) CE: 57.74 (b) SCE: 79.56 (c) MAE: 83.88

Figure 3: How Δ_y distributions of noisy (green, left) and clean (orange, right) samples change during training on CIFAR10 under symmetric label noise with $\eta = 0.4$. Vertical axes denoting probability density are scaled to the peak of histograms for better readability, with epoch number (axis scaling factor) denoted on the right of each subplot. We plot $w(\Delta_y)$ and report the test accuracy of each setting for reference. See Appendix C.2 for results with different label noise and more loss functions.

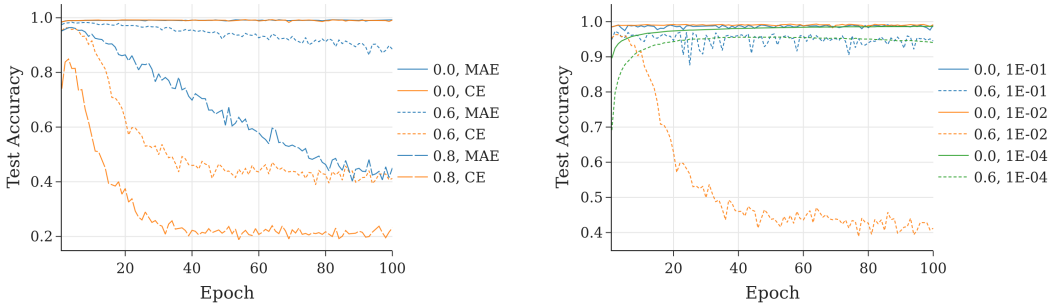

(a) $\alpha = 0.01$ with different (η, loss). (b) CE with different (η, α).

Figure 4: Learning curves with fixed learning rate and extended training epochs on MNIST under symmetric label noise, where α is the learning rate and η the noise rate.

distributions initially concentrate at the monotonically increasing interval of $w(\Delta_y)$, (1) samples with faster improving Δ_y, due to either larger initial weights or faster learning as clean samples, are weighted more during early training and learned faster. The magnified learning pace difference explains the widely spread distributions in Fig. 3b and 3c. In addition, (2) the unlearned samples with small Δ_y receive diminishing weights from $w(\Delta_y)$, which hampers their pace of learning. Noisy samples in Fig. 3b and 3c are consistently unlearned and ignored with marginal sample weights, leading to a consistent decrease in Δ_y. In addition to the SGD dynamics, (1) and (2) further suppress the learning of noisy samples and enhance that of clean samples, thus leading to increased robustness against label noise. In contrast, the monotonically decreasing $w_{\mathrm{CE}}(\Delta_y)$ emphasizes samples with smaller Δ_y, essentially acting against the SGD dynamics for noise robustness. Thus training with CE results in increased vulnerability to label noise as shown in Table 5.

4.2.1 Training Schedules Affect Noise Robustness

Although the learning pace of noisy samples gets initially suppressed, the expected gradient will eventually be dominated by noisy samples, since well-learned clean samples receive marginal sample weights thanks to the monotonically decreasing interval of $w(\Delta_y)$. Models with extended training[3] thus risk overfitting noisy samples during the late training stage. Adjusting the training schedules to enable or avoid such overfitting can therefore affect the noise robustness of models. Based on this hypothesis, we present two phenomenons on noise robustness as *examples* that follow our curriculum perspective but deviate from existing theoretical results:

[3]Enough training steps without early stopping or diminishing learning rates for a small training loss.

Extended training can make robust loss functions vulnerable to label noise. The learning curves of CE and MAE with *constant* learning rates on MNIST are shown in Fig. 4a. Despite the theoretically guaranteed noise robustness (Ghosh et al., 2017), similar to CE, with extended training, MAE eventually overfits noisy samples, resulting in vulnerability to label noise.

CE can become robust by adjusting the learning rate schedule. To avoid overfitting noisy samples, we can avoid learning when noisy samples dominate the expected gradient. It can be achieved with either early stopping (Song et al., 2019), or a constrained learning pace that prevents sufficient learning of clean samples, which avoids diminishing weights for them. We show the learning curve of CE using fixed learning rates under symmetric label noise on MNIST in Fig. 4b. By simply increasing or decreasing the learning rate, which strengthens the implicit regularization of SGD (Smith et al., 2021) or directly slows down the learning pace, CE can become robust against label noise.

5 Related Work

Our work is closely related to robust loss functions against label noise (Song et al., 2020). Most existing research (Ghosh et al., 2017; Zhang & Sabuncu, 2018; Wang et al., 2019c; Ma et al., 2020; Liu & Guo, 2020; Cheng et al., 2021; Feng et al., 2020; Zhou et al., 2021b) focuses on bounding the difference between risk minimizers obtained using noisy and clean data without considering the training dynamics. In contrast, with our novel curriculum perspective, we analyze the training dynamics with robust loss functions for reasons behind their underfitting issue and noise robustness. The underfitting problem has been heuristically mitigated with loss combination (Zhang & Sabuncu, 2018; Wang et al., 2019c; Ma et al., 2020). We identify the cause and provide an effective solution.

Curriculum-based approaches combat label noise with either sample selection (Chen et al., 2019; Zhou et al., 2021a) or sample weighting (Chang et al., 2017; Jiang et al., 2018; Ren et al., 2018). In particular, sample weights are *explicitly* designed (Wang et al., 2019a;b; Chang et al., 2017) or predicted by a model trained on a different dataset (Jiang et al., 2018; Ren et al., 2018). In contrast, the sample weights in this work are *implicitly* defined by robust loss functions. Notably, the implicit loss function we identified is a more direct metric for sample difficulty compared to loss functions (Kumar et al., 2010; Loshchilov & Hutter, 2015) and gradient magnitudes (Gopal, 2016), which are implicitly affected by the preference from the sample-weighting functions of loss functions.

Our work is also related to the ongoing debate (Hacohen & Weinshall, 2019; Wang et al., 2020) on strategies for selecting or weighting samples in curriculum learning: either easier first (Bengio et al., 2009; Kumar et al., 2010) or harder first (Loshchilov & Hutter, 2015; Zhang et al., 2018). The implicit curriculums of robust loss functions can be viewed as a combination of both strategies, emphasizing samples with moderate difficulty.

Most related to our work, Wang et al. (2019b) identify gradient norms as weights for sample gradients and propose heuristic designs of weighting functions for noise-robust training. In contrast, we explicitly identify the implicit loss function, which connects robust loss functions to curriculum learning, facilitates our analysis of the training dynamics and helps elucidate the robustness of loss functions from a curriculum perspective.

6 Conclusion and Discussions

We identified the implicit sample-weighting curriculums of a broad array of loss functions. Our novel curriculum perspective enables examining the training dynamics with loss functions through the interaction between the sample-weighting function and distributions of implicit losses. It connects robust loss functions to the seemingly distinct curriculum learning. Notably, the implicit loss function we identified is a direct metric for sample difficulty in curriculum learning as it factors out the preference of sample-weighting functions. We elucidate the reasons behind underfitting and robustness against label noise and propose a simple approach to address the underfitting issue.

As with previous work on robust loss functions, our empirical results are based on image classification using convolutional neural networks with and without residual connections. We have extended our experiments to cover larger-scale classification tasks, human label noise and a broader array of robust loss functions. Although our derivation does not depend on the models and task specifications, additional experiments should be performed in future work to extend our conclusions to more tasks and models.

REFERENCES

Devansh Arpit, Stanislaw Jastrzebski, Nicolas Ballas, David Krueger, Emmanuel Bengio, Maxinder S. Kanwal, Tegan Maharaj, Asja Fischer, Aaron C. Courville, Yoshua Bengio, and Simon Lacoste-Julien. A closer look at memorization in deep networks. In Doina Precup and Yee Whye Teh (eds.), *Proceedings of the 34th International Conference on Machine Learning, ICML 2017, Sydney, NSW, Australia, 6-11 August 2017*, volume 70 of *Proceedings of Machine Learning Research*, pp. 233–242. PMLR, 2017. URL http://proceedings.mlr.press/v70/arpit17a.html.

Jimmy Lei Ba, Jamie Ryan Kiros, and Geoffrey E. Hinton. Layer normalization, 2016. URL https://arxiv.org/abs/1607.06450.

Yoshua Bengio, Jérôme Louradour, Ronan Collobert, and Jason Weston. Curriculum learning. In Andrea Pohoreckyj Danyluk, Léon Bottou, and Michael L. Littman (eds.), *Proceedings of the 26th Annual International Conference on Machine Learning, ICML 2009, Montreal, Quebec, Canada, June 14-18, 2009*, volume 382 of *ACM International Conference Proceeding Series*, pp. 41–48. ACM, 2009. doi: 10.1145/1553374.1553380. URL https://doi.org/10.1145/1553374.1553380.

Pete Bridge, Andrew Fielding, Pamela Rowntree, and Andrew Pullar. Intraobserver variability: should we worry? *Journal of medical imaging and radiation sciences*, 47(3):217–220, 2016.

Haw-Shiuan Chang, Erik G. Learned-Miller, and Andrew McCallum. Active bias: Training more accurate neural networks by emphasizing high variance samples. In Isabelle Guyon, Ulrike von Luxburg, Samy Bengio, Hanna M. Wallach, Rob Fergus, S. V. N. Vishwanathan, and Roman Garnett (eds.), *Advances in Neural Information Processing Systems 30: Annual Conference on Neural Information Processing Systems 2017, December 4-9, 2017, Long Beach, CA, USA*, pp. 1002–1012, 2017. URL https://proceedings.neurips.cc/paper/2017/hash/2f37d10131f2a483a8dd005b3d14b0d9-Abstract.html.

Satrajit Chatterjee and Piotr Zielinski. On the generalization mystery in deep learning. *ArXiv preprint*, abs/2203.10036, 2022. URL https://arxiv.org/abs/2203.10036.

Pengfei Chen, Benben Liao, Guangyong Chen, and Shengyu Zhang. Understanding and utilizing deep neural networks trained with noisy labels. In Kamalika Chaudhuri and Ruslan Salakhutdinov (eds.), *Proceedings of the 36th International Conference on Machine Learning, ICML 2019, 9-15 June 2019, Long Beach, California, USA*, volume 97 of *Proceedings of Machine Learning Research*, pp. 1062–1070. PMLR, 2019. URL http://proceedings.mlr.press/v97/chen19g.html.

Hao Cheng, Zhaowei Zhu, Xingyu Li, Yifei Gong, Xing Sun, and Yang Liu. Learning with instance-dependent label noise: A sample sieve approach. In *9th International Conference on Learning Representations, ICLR 2021, Virtual Event, Austria, May 3-7, 2021*. OpenReview.net, 2021. URL https://openreview.net/forum?id=2VXyy9mIyU3.

Barry Cobb, Rafael Rumí, and Antonio Salmerón. Approximating the distribution of a sum of log-normal random variables. 2012.

Lei Feng, Senlin Shu, Zhuoyi Lin, Fengmao Lv, Li Li, and Bo An. Can cross entropy loss be robust to label noise? In Christian Bessiere (ed.), *Proceedings of the Twenty-Ninth International Joint Conference on Artificial Intelligence, IJCAI 2020*, pp. 2206–2212. ijcai.org, 2020. doi: 10.24963/ijcai.2020/305. URL https://doi.org/10.24963/ijcai.2020/305.

Aritra Ghosh, Himanshu Kumar, and P. S. Sastry. Robust loss functions under label noise for deep neural networks. In Satinder P. Singh and Shaul Markovitch (eds.), *Proceedings of the Thirty-First AAAI Conference on Artificial Intelligence, February 4-9, 2017, San Francisco, California, USA*, pp. 1919–1925. AAAI Press, 2017. URL http://aaai.org/ocs/index.php/AAAI/AAAI17/paper/view/14759.

Xavier Glorot and Yoshua Bengio. Understanding the difficulty of training deep feedforward neural networks. In *Proceedings of the Thirteenth International Conference on Artificial Intelligence and Statistics*, pp. 249–256. JMLR Workshop and Conference Proceedings, 2010. URL https://proceedings.mlr.press/v9/glorot10a.html.

Siddharth Gopal. Adaptive sampling for SGD by exploiting side information. In Maria-Florina Balcan and Kilian Q. Weinberger (eds.), *Proceedings of the 33nd International Conference on Machine Learning, ICML 2016, New York City, NY, USA, June 19-24, 2016*, volume 48 of *JMLR Workshop and Conference Proceedings*, pp. 364–372. JMLR.org, 2016. URL http://proceedings.mlr.press/v48/gopal16.html.

Guy Hacohen and Daphna Weinshall. On the power of curriculum learning in training deep networks. In Kamalika Chaudhuri and Ruslan Salakhutdinov (eds.), *Proceedings of the 36th International Conference on Machine Learning, ICML 2019, 9-15 June 2019, Long Beach, California, USA*, volume 97 of *Proceedings of Machine Learning Research*, pp. 2535–2544. PMLR, 2019. URL http://proceedings.mlr.press/v97/hacohen19a.html.

Bo Han, Quanming Yao, Xingrui Yu, Gang Niu, Miao Xu, Weihua Hu, Ivor W. Tsang, and Masashi Sugiyama. Co-teaching: Robust training of deep neural networks with extremely noisy labels. In Samy Bengio, Hanna M. Wallach, Hugo Larochelle, Kristen Grauman, Nicolò Cesa-Bianchi, and Roman Garnett (eds.), *Advances in Neural Information Processing Systems 31: Annual Conference on Neural Information Processing Systems 2018, NeurIPS 2018, December 3-8, 2018, Montréal, Canada*, pp. 8536–8546, 2018. URL https://proceedings.neurips.cc/paper/2018/hash/a19744e268754fb0148b017647355b7b-Abstract.html.

Kaiming He, Xiangyu Zhang, Shaoqing Ren, and Jian Sun. Delving deep into rectifiers: Surpassing human-level performance on imagenet classification. In *2015 IEEE International Conference on Computer Vision, ICCV 2015, Santiago, Chile, December 7-13, 2015*, pp. 1026–1034. IEEE Computer Society, 2015. doi: 10.1109/ICCV.2015.123. URL https://doi.org/10.1109/ICCV.2015.123.

Kaiming He, Xiangyu Zhang, Shaoqing Ren, and Jian Sun. Deep residual learning for image recognition. In *2016 IEEE Conference on Computer Vision and Pattern Recognition, CVPR 2016, Las Vegas, NV, USA, June 27-30, 2016*, pp. 770–778. IEEE Computer Society, 2016. doi: 10.1109/CVPR.2016.90. URL https://doi.org/10.1109/CVPR.2016.90.

Sergey Ioffe and Christian Szegedy. Batch normalization: Accelerating deep network training by reducing internal covariate shift. In Francis R. Bach and David M. Blei (eds.), *Proceedings of the 32nd International Conference on Machine Learning, ICML 2015, Lille, France, 6-11 July 2015*, volume 37 of *JMLR Workshop and Conference Proceedings*, pp. 448–456. JMLR.org, 2015. URL http://proceedings.mlr.press/v37/ioffe15.html.

Lu Jiang, Zhengyuan Zhou, Thomas Leung, Li-Jia Li, and Li Fei-Fei. Mentornet: Learning data-driven curriculum for very deep neural networks on corrupted labels. In Jennifer G. Dy and Andreas Krause (eds.), *Proceedings of the 35th International Conference on Machine Learning, ICML 2018, Stockholmsmässan, Stockholm, Sweden, July 10-15, 2018*, volume 80 of *Proceedings of Machine Learning Research*, pp. 2309–2318. PMLR, 2018. URL http://proceedings.mlr.press/v80/jiang18c.html.

Yoshihide Kato and Shigeki Matsubara. Correcting errors in a treebank based on synchronous tree substitution grammar. In *Proceedings of the ACL 2010 Conference Short Papers*, pp. 74–79, Uppsala, Sweden, 2010. Association for Computational Linguistics. URL https://aclanthology.org/P10-2014.

Huda Khayrallah and Philipp Koehn. On the impact of various types of noise on neural machine translation. In *Proceedings of the 2nd Workshop on Neural Machine Translation and Generation*, pp. 74–83, Melbourne, Australia, 2018. Association for Computational Linguistics. doi: 10.18653/v1/W18-2709. URL https://aclanthology.org/W18-2709.

Alex Krizhevsky. Learning multiple layers of features from tiny images. Technical report, 2009.

M. Pawan Kumar, Benjamin Packer, and Daphne Koller. Self-paced learning for latent variable models. In John D. Lafferty, Christopher K. I. Williams, John Shawe-Taylor, Richard S. Zemel, and Aron Culotta (eds.), *Advances in Neural Information Processing Systems 23: 24th Annual Conference on Neural Information Processing Systems 2010. Proceedings of a meeting held 6-9 December 2010, Vancouver, British Columbia, Canada*, pp. 1189–1197. Curran Associates, Inc., 2010. URL https://proceedings.neurips.cc/paper/2010/hash/e57c6b956a6521b28495f2886ca0977a-Abstract.html.

Y. Lecun, L. Bottou, Y. Bengio, and P. Haffner. Gradient-based learning applied to document recognition. *Proceedings of the IEEE*, 86(11):2278–2324, 1998. doi: 10.1109/5.726791.

Wen Li, Limin Wang, Wei Li, Eirikur Agustsson, and Luc Van Gool. Webvision database: Visual learning and understanding from web data, 2017. URL https://arxiv.org/abs/1708.02862.

Tsung-Yi Lin, Priya Goyal, Ross B. Girshick, Kaiming He, and Piotr Dollár. Focal loss for dense object detection. In *IEEE International Conference on Computer Vision, ICCV 2017, Venice, Italy, October 22-29, 2017*, pp. 2999–3007. IEEE Computer Society, 2017. doi: 10.1109/ICCV.2017.324. URL https://doi.org/10.1109/ICCV.2017.324.

Kun Liu, Yao Fu, Chuanqi Tan, Mosha Chen, Ningyu Zhang, Songfang Huang, and Sheng Gao. Noisy-labeled NER with confidence estimation. In *Proceedings of the 2021 Conference of the North American Chapter of the Association for Computational Linguistics: Human Language Technologies*, pp. 3437–3445, Online, 2021. Association for Computational Linguistics. doi: 10.18653/v1/2021.naacl-main.269. URL https://aclanthology.org/2021.naacl-main.269.

Yang Liu and Hongyi Guo. Peer loss functions: Learning from noisy labels without knowing noise rates. In *Proceedings of the 37th International Conference on Machine Learning, ICML 2020, 13-18 July 2020, Virtual Event*, volume 119 of *Proceedings of Machine Learning Research*, pp. 6226–6236. PMLR, 2020. URL http://proceedings.mlr.press/v119/liu20e.html.

Ilya Loshchilov and Frank Hutter. Online batch selection for faster training of neural networks. *ArXiv preprint*, abs/1511.06343, 2015. URL https://arxiv.org/abs/1511.06343.

Michal Lukasik, Srinadh Bhojanapalli, Aditya Krishna Menon, and Sanjiv Kumar. Does label smoothing mitigate label noise? In *Proceedings of the 37th International Conference on Machine Learning, ICML 2020, 13-18 July 2020, Virtual Event*, volume 119 of *Proceedings of Machine Learning Research*, pp. 6448–6458. PMLR, 2020. URL http://proceedings.mlr.press/v119/lukasik20a.html.

Xingjun Ma, Hanxun Huang, Yisen Wang, Simone Romano, Sarah M. Erfani, and James Bailey. Normalized loss functions for deep learning with noisy labels. In *Proceedings of the 37th International Conference on Machine Learning, ICML 2020, 13-18 July 2020, Virtual Event*, volume 119 of *Proceedings of Machine Learning Research*, pp. 6543–6553. PMLR, 2020. URL http://proceedings.mlr.press/v119/ma20c.html.

Giorgio Patrini, Alessandro Rozza, Aditya Krishna Menon, Richard Nock, and Lizhen Qu. Making deep neural networks robust to label noise: A loss correction approach. In *2017 IEEE Conference on Computer Vision and Pattern Recognition, CVPR 2017, Honolulu, HI, USA, July 21-26, 2017*, pp. 2233–2241. IEEE Computer Society, 2017. doi: 10.1109/CVPR.2017.240. URL https://doi.org/10.1109/CVPR.2017.240.

Mengye Ren, Wenyuan Zeng, Bin Yang, and Raquel Urtasun. Learning to reweight examples for robust deep learning. In Jennifer G. Dy and Andreas Krause (eds.), *Proceedings of the 35th International Conference on Machine Learning, ICML 2018, Stockholmsmässan, Stockholm, Sweden, July 10-15, 2018*, volume 80 of *Proceedings of Machine Learning Research*, pp. 4331–4340. PMLR, 2018. URL http://proceedings.mlr.press/v80/ren18a.html.

Olga Russakovsky, Jia Deng, Hao Su, Jonathan Krause, Sanjeev Satheesh, Sean Ma, Zhiheng Huang, Andrej Karpathy, Aditya Khosla, Michael Bernstein, Alexander C. Berg, and Li Fei-Fei. Imagenet large scale visual recognition challenge. *arXiv:1409.0575 [cs]*, 2015. URL http://arxiv.org/abs/1409.0575. arXiv: 1409.0575.

Samuel L. Smith, Benoit Dherin, David G. T. Barrett, and Soham De. On the origin of implicit regularization in stochastic gradient descent. In *9th International Conference on Learning Representations, ICLR 2021, Virtual Event, Austria, May 3-7, 2021*. OpenReview.net, 2021. URL https://openreview.net/forum?id=rq_Qr0c1Hyo.

Hwanjun Song, Minseok Kim, Dongmin Park, and Jae-Gil Lee. How does early stopping help generalization against label noise?, 2019. URL https://arxiv.org/abs/1911.08059.

Hwanjun Song, Minseok Kim, Dongmin Park, Yooju Shin, and Jae-Gil Lee. Learning from noisy labels with deep neural networks: A survey. *ArXiv preprint*, abs/2007.08199, 2020. URL https://arxiv.org/abs/2007.08199.

Christian Szegedy, Vincent Vanhoucke, Sergey Ioffe, Jonathon Shlens, and Zbigniew Wojna. Rethinking the inception architecture for computer vision. In *2016 IEEE Conference on Computer Vision and Pattern Recognition, CVPR 2016, Las Vegas, NV, USA, June 27-30, 2016*, pp. 2818–2826. IEEE Computer Society, 2016. doi: 10.1109/CVPR.2016.308. URL https://doi.org/10.1109/CVPR.2016.308.

Yee Whye Teh, David Newman, and Max Welling. A collapsed variational bayesian inference algorithm for latent dirichlet allocation. In Bernhard Schölkopf, John C. Platt, and Thomas Hofmann (eds.), *Advances in Neural Information Processing Systems 19, Proceedings of the Twentieth Annual Conference on Neural Information Processing Systems, Vancouver, British Columbia, Canada, December 4-7, 2006*, pp. 1353–1360. MIT Press, 2006. URL https://proceedings.neurips.cc/paper/2006/hash/532b7cbe070a3579f424988a040752f2-Abstract.html.

Xin Wang, Yudong Chen, and Wenwu Zhu. A survey on curriculum learning. *ArXiv preprint*, abs/2010.13166, 2020. URL https://arxiv.org/abs/2010.13166.

Xinshao Wang, Yang Hua, Elyor Kodirov, and Neil M. Robertson. Imae for noise-robust learning: Mean absolute error does not treat examples equally and gradient magnitude's variance matters. *ArXiv preprint*, abs/1903.12141, 2019a. URL https://arxiv.org/abs/1903.12141.

Xinshao Wang, Elyor Kodirov, Yang Hua, and Neil M. Robertson. Derivative manipulation for general example weighting. *ArXiv preprint*, abs/1905.11233, 2019b. URL https://arxiv.org/abs/1905.11233.

Yisen Wang, Xingjun Ma, Zaiyi Chen, Yuan Luo, Jinfeng Yi, and James Bailey. Symmetric cross entropy for robust learning with noisy labels. In *2019 IEEE/CVF International Conference on Computer Vision, ICCV 2019, Seoul, Korea (South), October 27 - November 2, 2019*, pp. 322–330. IEEE, 2019c. doi: 10.1109/ICCV.2019.00041. URL https://doi.org/10.1109/ICCV.2019.00041.

Jiaheng Wei, Hangyu Liu, Tongliang Liu, Gang Niu, Masashi Sugiyama, and Yang Liu. To smooth or not? when label smoothing meets noisy labels. *ArXiv preprint*, abs/2106.04149, 2021. URL https://arxiv.org/abs/2106.04149.

Jiaheng Wei, Zhaowei Zhu, Hao Cheng, Tongliang Liu, Gang Niu, and Yang Liu. Learning with noisy labels revisited: A study using real-world human annotations. In *International Conference on Learning Representations*, 2022. URL https://openreview.net/forum?id=TBWA6PLJZQm.

Quanming Yao, Hansi Yang, Bo Han, Gang Niu, and James Kwok. Searching to exploit memorization effect in learning from corrupted labels, 2019. URL https://arxiv.org/abs/1911.02377.

Chiyuan Zhang, Samy Bengio, Moritz Hardt, Benjamin Recht, and Oriol Vinyals. Understanding deep learning requires rethinking generalization. In *5th International Conference on Learning Representations, ICLR 2017, Toulon, France, April 24-26, 2017, Conference Track Proceedings*. OpenReview.net, 2017. URL https://openreview.net/forum?id=Sy8gdB9xx.

Xuan Zhang, Gaurav Kumar, Huda Khayrallah, Kenton Murray, Jeremy Gwinnup, Marianna J. Martindale, Paul McNamee, Kevin Duh, and Marine Carpuat. An empirical exploration of curriculum learning for neural machine translation. *ArXiv preprint*, abs/1811.00739, 2018. URL https://arxiv.org/abs/1811.00739.

Zhilu Zhang and Mert R. Sabuncu. Generalized cross entropy loss for training deep neural networks with noisy labels. In Samy Bengio, Hanna M. Wallach, Hugo Larochelle, Kristen Grauman, Nicolò Cesa-Bianchi, and Roman Garnett (eds.), *Advances in Neural Information Processing Systems 31: Annual Conference on Neural Information Processing Systems 2018, NeurIPS 2018, December 3-8, 2018, Montréal, Canada*, pp.

8792–8802, 2018. URL https://proceedings.neurips.cc/paper/2018/hash/f2925f97bc13ad2852a7a551802feea0-Abstract.html.

Tianyi Zhou, Shengjie Wang, and Jeff A. Bilmes. Robust curriculum learning: from clean label detection to noisy label self-correction. In *9th International Conference on Learning Representations, ICLR 2021, Virtual Event, Austria, May 3-7, 2021*. OpenReview.net, 2021a. URL https://openreview.net/forum?id=lmTWnm3coJJ.

Xiong Zhou, Xianming Liu, Junjun Jiang, Xin Gao, and Xiangyang Ji. Asymmetric loss functions for learning with noisy labels. In Marina Meila and Tong Zhang (eds.), *Proceedings of the 38th International Conference on Machine Learning, ICML 2021, 18-24 July 2021, Virtual Event*, volume 139 of *Proceedings of Machine Learning Research*, pp. 12846–12856. PMLR, 2021b. URL http://proceedings.mlr.press/v139/zhou21f.html.

A Extended Review of Loss Functions

Due to limited space, we only briefly describe typical robust loss functions in §2.1. As a general reference, here we provide a comprehensive review of loss functions related to the standard form Eq. (6). Similar to §2.1, we ignore the differences in constant scaling factors and additive bias. Loss functions and their sample-weighting functions are summarized in Table 6. We examine how hyperparameters affect their sample-weighting functions in Fig. 5.

A.1 Loss Functions without Robustness Guarantees

Cross Entropy (CE)

$$L_{\mathrm{CE}}(\boldsymbol{s}, y) = -\log p_y$$

is the standard loss function for classification.

Focal Loss (FL; Lin et al. 2017)

$$L_{\mathrm{FL}}(\boldsymbol{s}, y) = -(1-p_y)^q \log p_y$$

aims to address label imbalance when training object detection models. Both CE and FL are neither symmetric (Ma et al., 2020) nor asymmetric (Zhou et al., 2021b).

A.2 Symmetric Loss Functions

Mean Absolute Error (MAE; Ghosh et al. 2017)

$$L_{\mathrm{MAE}}(\boldsymbol{s}, y) = \sum_{i=1}^{k} |\mathbb{I}(i=y) - p_i| = 2 - 2p_y \propto 1 - p_y$$

is a classic symmetric loss function, where $\mathbb{I}(i=y)$ is the indicator function.

Reverse Cross Entropy (RCE; Wang et al. 2019c)

$$L_{\mathrm{RCE}}(\boldsymbol{s}, y) = \sum_{i=1}^{k} p_i \log \mathbf{1}(i=y) = \sum_{i \neq y} p_i A = (1-p_y)A \propto 1 - p_y = L_{\mathrm{MAE}}(\boldsymbol{s}, y)$$

is equivalent to MAE in implementation, where $\log 0$ is truncated to a negative constant A to avoid numerical overflow.

Ma et al. (2020) argued that any generic loss functions with $L(\boldsymbol{s}, i) > 0, \forall i \in \{1..k\}$ can become symmetric by simply normalizing them. As an example,

Normalized Cross Entropy (NCE; Ma et al. 2020)

$$L_{\mathrm{NCE}}(\boldsymbol{s}, y) = \frac{L_{\mathrm{CE}}(\boldsymbol{s}, y)}{\sum_{i=1}^{k} L_{\mathrm{CE}}(\boldsymbol{s}, i)} = \frac{-\log p_y}{\sum_{i=1}^{k} -\log p_i}$$

is a symmetric loss function. However, NCE does not follow the standard form of Eq. (6) as it additionally depends on p_i, $i \neq y$. It involves an additional regularizer, thus being more relevant to discussions in Appendix A.5.

Name	Function	Sample Weight w	Constraints
CE	$-\log p_y$	$1-p_y$	
FL	$-(1-p_y)^q \log p_y$	$(1-p_y)^q(1-p_y-qp_y\log p_y)$	$q>0$
MAE/RCE	$1-p_y$	$p_y(1-p_y)$	
AUL	$\frac{(a+1)-(a+p_y)^q}{q}$	$p_y(1-p_y)(a-p_y)^{q-1}$	$a>1, q>0$
AGCE	$\frac{(a-p_y)^q-(a-1)^q}{q}$	$p_y(a+p_y)^{q-1}(1-p_y)$	$a>0, q>0$
AEL	$e^{-p_y/q}$	$\frac{1}{q}p_y(1-p_y)e^{-p_y/q}$	$q>0$
GCE	$(1-p_y^q)/q$	$p_y^q(1-p_y)$	$0<q\leq 1$
SCE	$-(1-q)\log p_y + q(1-p_y)$	$(1-q+q\cdot p_y)(1-p_y)$	$0<q<1$
TCE	$\sum_{i=1}^{q}(1-p_y)^i/i$	$p_y\sum_{i=1}^{q}(1-p_y)^i$	$q\geq 1$

Table 6: Expressions, constraints of hyperparameters and sample-weighting functions of loss functions reviewed in Appendix A that follow the standard form Eq. (6).

A.3 Asymmetric Loss Functions

Zhou et al. (2021b) derived the asymmetric condition for noise robustness and propose numerous asymmetric loss functions:

Asymmetric Generalized Cross Entropy (AGCE)

$$L_{\mathrm{AGCE}}(\boldsymbol{s}, y) = \frac{(a+1)-(a+p_y)^q}{q}$$

where $a>0$ and $q>0$. It is asymmetric when $\mathbb{I}(q\leq 1)(\frac{a+1}{a})^{1-q} + \mathbb{I}(q>1) \leq 1/\tilde{r}$.

Asymmetric Unhinged Loss (AUL)

$$L_{\mathrm{AUL}}(\boldsymbol{s}, y) = \frac{(a-p_y)^q-(a-1)^q}{q}$$

where $a>1$ and $q>0$. It is asymmetric when $\mathbb{I}(q\leq 1)(\frac{a}{a-1})^{q-1} + \mathbb{I}(q\leq 1) \leq 1/\tilde{r}$.

Asymmetric Exponential Loss (AEL)

$$L_{\mathrm{AEL}}(\boldsymbol{s}, y) = e^{-p_y/q}$$

where $q>0$. It is asymmetric when $e^{1/q}\leq 1/\tilde{r}$.

A.4 Combined Loss Functions

Generalized Cross Entropy (GCE; Zhang & Sabuncu 2018)

$$L_{\mathrm{GCE}}(\boldsymbol{s}, y) = \frac{1-p_y^q}{q}$$

can be viewed as a smooth interpolation between CE and MAE, where $0<q\leq 1$. CE or MAE can be recovered by setting $q\to 0$ or $q=1$.

Symmetric Cross Entropy (SCE; Wang et al. 2019c)

$$\begin{aligned} L_{\mathrm{SCE}}(\boldsymbol{s}, y) &= a\cdot L_{\mathrm{CE}}(\boldsymbol{s}, y) + b\cdot L_{\mathrm{RCE}}(\boldsymbol{s}, y) \\ &\propto (1-q)\cdot(-\log p_i) + q\cdot(1-p_i) \end{aligned}$$

is a weighted average of CE and RCE (MAE), where $a>0$, $b>0$, and $0<q<1$.

Taylor Cross Entropy (TCE; Feng et al. 2020)

$$L_{\mathrm{TCE}}(\boldsymbol{s}, y) = \sum_{i=1}^{q}\frac{(1-p_y)^i}{i}$$

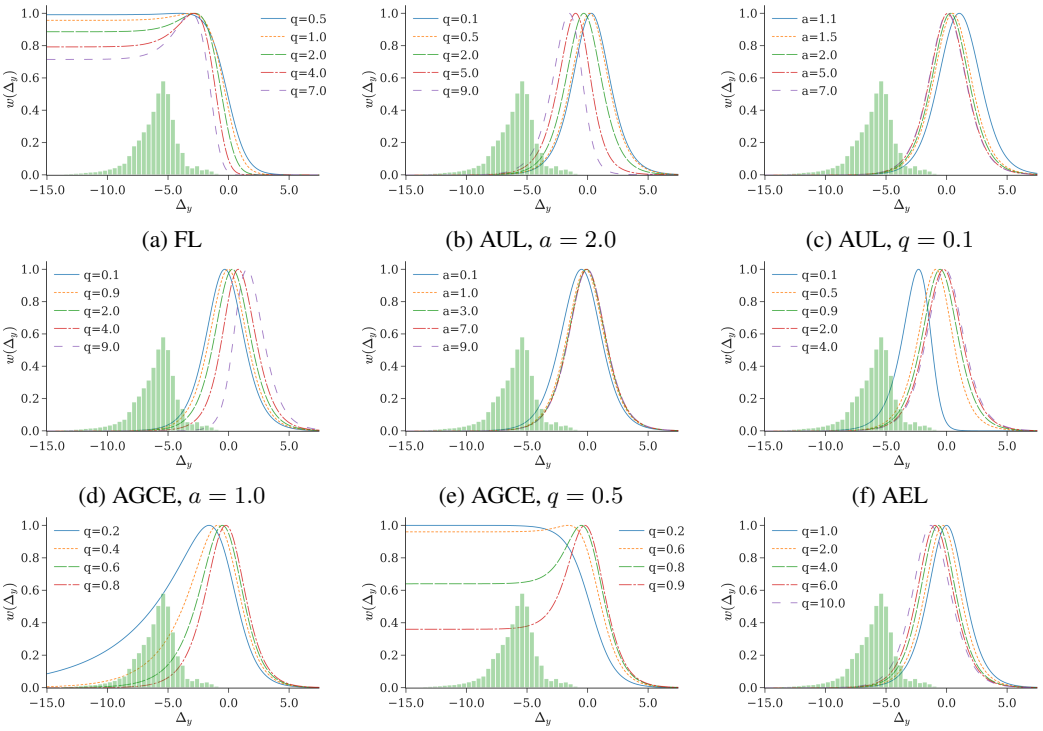

(a) FL (b) AUL, $a = 2.0$ (c) AUL, $q = 0.1$

(d) AGCE, $a = 1.0$ (e) AGCE, $q = 0.5$ (f) AEL

(g) GCE (h) SCE (i) TCE

Figure 5: How hyperparameters affect the sample-weighting functions in Table 6. The initial Δ_y distributions of CIFAR100 extracted with a randomly initialized model are included as reference.

is derived from Taylor series of the $\log$ function. It reduces to MAE when $q = 1$. Interestingly, the summand of TCE $(1 - p_y)^i/i$ with $i > 2$ is proportional to AUL with $a = 1$ and $q = i$. Thus TCE can be viewed as a combination of symmetric and asymmetric loss functions.

Active-Passive Loss (APL; Ma et al. 2020)

Ma et al. (2020) propose weighted combinations of active and passive loss functions. We include NCE+MAE as an example:

$$L_{\text{NCE+MAE}}(\boldsymbol{s}, y) = a \cdot L_{\text{NCE}}(\boldsymbol{s}, y) + b \cdot L_{\text{MAE}}(\boldsymbol{s}, y)$$
$$\propto (1 - q) \cdot \frac{-\log p_y}{\sum_{i=1}^{k} -\log p_i} + q \cdot (1 - p_y)$$

where $a > 0$, $b > 0$, and $0 < q < 1$.

A.5 Loss Functions with Additional Regularizers

We additionally review loss functions that implicitly involve a regularizer and a primary loss function following the standard form Eq. (6). See Table 7 for a summary. We leave investigations on how these additional regularizers affect noise robustness for future work.

Mean Square Error (MSE; Ghosh et al. 2017)

$$L_{\text{MSE}}(\boldsymbol{s}, y) = \sum_{i=1}^{k} (\mathbb{I}(i = y) - p_i)^2 = 1 - 2p_y + \sum_{i=1}^{k} p_i^2$$
$$\propto 1 - p_y + \frac{1}{2} \cdot \sum_{i=1}^{k} p_i^2 = L_{\text{MAE}}(\boldsymbol{s}, y) + \alpha \cdot R_{\text{MSE}}(\boldsymbol{s})$$

is more robust than CE (Ghosh et al., 2017), where $\alpha = 0.5$ and the regularizer

$$R_{\text{MSE}}(\boldsymbol{s}) = \sum_{i=1}^{k} p_i^2 \tag{10}$$

Name	Original	Primary Loss	Regularizer
MSE	$1 - 2p_y + \sum_{i=1}^k p_i^2$	$1 - p_y$	$\sum_{i=1}^k p_i^2$
PL(CR)	$-\log p_y + \log p_{y_n \mid \boldsymbol{x}_m}$	$-\log p_y$	$\sum_{i=1}^k P(\tilde{y} = i) \log p_i$
CE+GLS	$-\sum_{i=1}^k [\mathbb{I}(i = y)(1-\alpha) + \frac{\alpha}{k}] \log p_i$	$-\log p_y$	$\pm \sum_{i=1}^k \frac{1}{k} \log p_i$
NCE	$-\log p_y / (\sum_{i=1}^k - \log p_i)$	$-\gamma_{\text{NCE}} \cdot \log p_i$	$\sum_{i=1}^k \frac{1}{k} \log p_i$

Table 7: Original expressions, primary loss functions in the standard form Eq. (6) and regularizers for loss functions reviewed in Appendix A.5. We view PL in its expectation to derive its regularizer. $p_{y_n \mid \boldsymbol{x}_m}$ is the softmax probability of a random label y_n with a random input $\boldsymbol{x}_m$ sampled from the noisy data. $\gamma_{\text{NCE}} = 1/(\sum_{i=1}^k - \log p_i)$ is a scalar wrapped with the stop-gradient operator.

increases the entropy of the softmax output. We can generalize α to a hyperparamter, making MSE a combination of MAE and an entropy regularizer R_{MSE}.

Peer Loss (PL; Liu & Guo 2020)

$$L_{\text{PL}}(\boldsymbol{s}, y) = L(\boldsymbol{s}, y) - L(\boldsymbol{s}_n, y_m)$$

makes a generic loss function $L(\boldsymbol{s}, y)$ robust against label noise, where $\boldsymbol{s}_n$ denotes the score of an input $\boldsymbol{x}_n$ and y_m a label, both randomly sampled from the noisy data. Its noise robustness is theoretically established for binary classification and extended to multi-class setting (Liu & Guo, 2020).

Confidence Regularizer (CR; Cheng et al. 2021)

$$R_{\text{CR}}(\boldsymbol{s}) = -\mathbb{E}_{\tilde{y}}[L(\boldsymbol{s}, \tilde{y})]$$

is shown (Cheng et al., 2021) to be the regularizer induced by PL in expectation. Substituting L with cross entropy leads to

$$R_{\text{CR}}(\boldsymbol{s}) = -\mathbb{E}_{\tilde{y}}[-\log p_{\tilde{y}}] = \sum_{i=1}^k P(\tilde{y} = i) \log p_i \tag{11}$$

Minimizing $R_{\text{CR}}(\boldsymbol{s})$ thus makes the softmax output distribution $\boldsymbol{p}$ deviate from the prior label distribution of the noisy dataset $P(\tilde{y} = i)$, reducing the entropy of the softmax output.

Generalized Label Smoothing (GLS; Wei et al. 2021)

Lukasik et al. (2020) show that label smoothing (LS; Szegedy et al. 2016) can mitigate overfitting with label noise, which is later extended to GSL. Cross entropy with GLS is

$$\begin{aligned} L_{\text{CE+GLS}}(\boldsymbol{s}, y) &= \sum_{i=1}^k -[\mathbb{I}(i = y)(1-\alpha) + \frac{\alpha}{k}] \log p_i \\ &= -(1-\alpha) \log p_y - \alpha \cdot \frac{1}{k} \sum_{i=1}^k \log p_i \\ &\propto -\log p_y - \frac{\alpha}{1-\alpha} \cdot \frac{1}{k} \sum_{i=1}^k \log p_i = L_{\text{CE}}(\boldsymbol{s}, y) + \alpha' \cdot R_{\text{GLS}}(\boldsymbol{s}) \end{aligned}$$

where $\alpha' = \alpha/(1-\alpha)$, has regularizer R_{GLS}

$$R_{\text{GLS}}(\boldsymbol{s}) = -\sum_{i=1}^k \frac{1}{k} \log p_i \tag{12}$$

With $\alpha' > 0$, R_{GLS} corresponds to the original label smoothing, which increases the entropy of softmax outputs. In contrast, $\alpha' < 0$ corresponding to negative label smoothing (Wei et al., 2021), which decreases the output entropy similar to R_{CR}.

A.5.1 DERIVATIONS FOR NCE

Deriving Eq. (7) With equivalent derivatives, since

$$\begin{aligned}\nabla_{\boldsymbol{s}} L_{\mathrm{NCE}}(\boldsymbol{s}, y) &= \frac{\nabla_{\boldsymbol{s}} L_{\mathrm{CE}}(\boldsymbol{s}, y) \cdot \left[\sum_{i=1}^{k} L_{\mathrm{CE}}(\boldsymbol{s}, i)\right] - \nabla_{\boldsymbol{s}} \left[\sum_{i=1}^{k} L_{\mathrm{CE}}(\boldsymbol{s}, i)\right] \cdot L_{\mathrm{CE}}(\boldsymbol{s}, y)}{\left[\sum_{i=1}^{k} L_{\mathrm{CE}}(\boldsymbol{s}, i)\right]^2} \\ &= \frac{1}{\sum_{i=1}^{k} L_{\mathrm{CE}}(\boldsymbol{s}, i)} \left\{ \nabla_{\boldsymbol{s}} L_{\mathrm{CE}}(\boldsymbol{s}, y) + \frac{k L_{\mathrm{CE}}(\boldsymbol{s}, y)}{\sum_{i=1}^{k} L_{\mathrm{CE}}(\boldsymbol{s}, i)} \cdot \nabla_{\boldsymbol{s}} \left[\sum_{i=1}^{k} -\frac{1}{k} L_{\mathrm{CE}}(\boldsymbol{s}, i)\right] \right\} \\ &= \gamma_{\mathrm{NCE}} \cdot \left[\nabla_{\boldsymbol{s}} L_{\mathrm{CE}}(\boldsymbol{s}, y) + \epsilon_{\mathrm{NCE}} \cdot \nabla_{\boldsymbol{s}} R_{\mathrm{NCE}}(\boldsymbol{s})\right],\end{aligned}$$

NCE can be rewritten as

$$L_{\mathrm{NCE}}(\boldsymbol{s}, y) = \gamma_{\mathrm{NCE}} \cdot L_{\mathrm{CE}}(\boldsymbol{s}, y) + \gamma_{\mathrm{NCE}} \cdot \epsilon_{\mathrm{NCE}} \cdot R_{\mathrm{NCE}}(\boldsymbol{s})$$

where $\gamma_{\mathrm{NCE}} = 1/(\sum_{i=1}^{k} -\log p_i)$ and $\epsilon_{\mathrm{NCE}} = k(-\log p_y)/(\sum_{i=1}^{k} -\log p_i)$ are scalar weights wrapped with the stop-gradient operator as discussed in §3.1. The regularizer

$$R_{\mathrm{NCE}}(\boldsymbol{s}) = \sum_{i=1}^{k} \frac{1}{k} \log p_i$$

has a form similar to R_{GLS}.

Deriving $\hat{w}_{\mathrm{NCE}}$ of Eq. (8) Here we derive the upperbound of $\|\nabla_{\boldsymbol{s}} L_{\mathrm{NCE}}(\boldsymbol{s}, y)\|_1$ discussed in §3.1:

$$\begin{aligned}\|\nabla_{\boldsymbol{s}} L_{\mathrm{NCE}}(\boldsymbol{s}, y)\|_1 &\leq \gamma_{\mathrm{NCE}} \cdot (\|\nabla_{\boldsymbol{s}} L_{\mathrm{CE}}(\boldsymbol{s}, y)\|_1 + \epsilon_{\mathrm{NCE}} \cdot \|\nabla_{\boldsymbol{s}} R_{\mathrm{NCE}}(\boldsymbol{s})\|_1) \\ &\leq \gamma_{\mathrm{NCE}} \cdot \left(\|\nabla_{\boldsymbol{s}} L_{\mathrm{CE}}(\boldsymbol{s}, y)\|_1 + \epsilon_{\mathrm{NCE}} \cdot \frac{1}{k} \sum_{i=1}^{k} \|\nabla_{\boldsymbol{s}} L_{\mathrm{CE}}(\boldsymbol{s}, i)\|_1 \right) \\ &= \gamma_{\mathrm{NCE}} \cdot \left(w_{\mathrm{CE}} \cdot \|\nabla_{\boldsymbol{s}} \Delta_y\|_1 + \epsilon_{\mathrm{NCE}} \cdot \frac{1}{k} \sum_{i=1}^{k} w_{\mathrm{CE}} \cdot \|\nabla_{\boldsymbol{s}} \Delta_i\|_1 \right) \\ &= 2\gamma_{\mathrm{NCE}} \cdot w_{\mathrm{CE}} \left(1 + \epsilon_{\mathrm{NCE}}\right) \\ &= \hat{w}_{\mathrm{NCE}}\end{aligned}$$

The derivation is based on the inequality $|x \pm y| \leq |x| + |y|$ and the fact that $\|\nabla_{\boldsymbol{s}} \Delta_i\|_1 = 2$. The latter can be proved by straightforward calculations. Given

$$\frac{\partial \Delta_i}{\partial s_j} = \begin{cases} 1, & j = i \\ -\frac{e^{s_j}}{\sum_{k \neq i} e^{s_k}} = -\frac{p_j}{1 - p_i}, & j \neq i \end{cases}$$

we then have

$$\|\nabla_{\boldsymbol{s}} \Delta_i\|_1 = \sum_j \left|\frac{\partial \Delta_i}{\partial s_j}\right| = 1 + \sum_{j \neq i} \frac{p_j}{1 - p_i} = 1 + 1 = 2$$

B DETAILED EXPERIMENTAL SETTINGS

Label noise The synthetic noisy labels are generated following (Ma et al., 2020; Zhou et al., 2021b; Patrini et al., 2017). For symmetric label noise, the training labels are randomly flipped to a different class with probabilities $\eta \in \{0.2, 0.4, 0.6, 0.8\}$. Asymmetric label noise is generated from a class-dependent flipping pattern. On CIFAR100, the 100 classes are grouped into 20 super-classes, each having 5 sub-classes. Each class is flipped within the same super-class into the next in a circular fashion. The flip probabilities are $\eta \in \{0.1, 0.2, 0.3, 0.4\}$. Human label noise for CIFAR10/100 are adopted from Wei et al. (2022). We use the "worst" labels of CIFAR10-N and the "fine" labels of CIFAR100-N, both leading to $\eta = 0.4$.

Models and hyperparameters We use a 4-layer CNN for MNIST, an 8-layer CNN for CIFAR10, a ResNet-34 (He et al., 2016) for CIFAR100, and a ResNet-50 (He et al., 2016) for WebVision, all with batch normalization (Ioffe & Szegedy, 2015). Data augmentation on CIFAR10/100 include random width/height shift and horizontal flip. On WebVision, we additionally include random cropping and

	SCE	GCE	NCE+MAE	AUL	AGCE	AUL†	AGCE†
a	/	/	/	1.1	0.1	3.0	1.6
q	0.7	0.3	0.3	5.0	0.1	0.7	2.0

Table 8: Hyperparameters of different loss functions for results in §4.1 and Appendix C.1. They are tuned on CIFAR100 without label noise. Settings with inferior hyperparameters are denoted with †.

Underfitting	Loss	CIFAR100 Acc.	CIFAR100 $\bar{\alpha}_t^*$	CIFAR10 Acc.	CIFAR10 $\bar{\alpha}_t^*$
/	CE	68.76 ± 0.21	0.962	90.24 ± 0.14	0.624
No	SCE	68.89 ± 0.05	1.165	91.07 ± 0.09	0.726
	GCE	69.00 ± 0.24	0.956	90.83 ± 0.20	0.644
	NCE+MAE	68.21 ± 0.51	/	90.14 ± 0.09	/
Moderate	AUL	47.98 ± 3.48	0.485	88.94 ± 0.29	0.604
	AGCE	43.51 ± 2.58	0.406	90.71 ± 0.19	0.549
	NCE	57.95 ± 0.26	/	85.96 ± 0.21	/
Severe	MAE	9.11 ± 0.83	0.025	90.65 ± 0.10	0.355
	AUL†	10.04 ± 2.33	0.023	90.77 ± 0.04	0.337
	AGCE†	5.34 ± 0.67	0.008	81.59 ± 8.55	0.243

Table 9: Similar results as Table 2 with learning rate $\alpha = 0.01$. Hyperparameters for loss functions are listed in Table 8.

color jittering. Without further specifications, all models are trained using SGD with momentum 0.9 and batch size 128 for 50, 120, 200 and 250 epochs on MNIST, CIFAR10, CIFAR100 and WebVision, respectively. Learning rates with cosine annealing are 0.01 on MNIST and CIFAR10, 0.1 on CIFAR100, and 0.2 on WebVision. Weight decays are 10^{-3} on MNIST, 10^{-4} on CIFAR10, 10^{-5} on CIFAR100 and 3×10^{-5} on WebVision. All loss functions are normalized to have unit maximum in sample weights, which is different from (Ma et al., 2020). Hyperparameters of loss functions are listed in Tables 8 and 13 for different experiments.

C Additional Results to Understand Robust Loss Functions

We complement §4 in the main text with detailed derivations and additional results. Appendix C.1 extends discussions in §4.1 while Appendix C.2 extends §4.2

C.1 Understanding Underfitting of Robust Loss Functions

Hyperparameters We list the hyperparameters tuned on CIFAR100 without label noise in Table 8 for experiments in §4.1 and Appendix C.1.

Robust loss functions can underfit. In Table 9 we report results similar to Table 2 with learning rate $\alpha = 0.01$. Although settings that severe underfit slightly improve, they still perform much worse than CE, which further confirms that underfitting results from robust loss functions themselves.

Simulated Δ_y approximate real settings. We compare the simulated Δ_y distributions based on our assumptions in §4.1 to distributions of real datasets at initialization in Fig. 6. The expectations of simulated Δ_y follow real settings, which supports the analysis in §4.1.

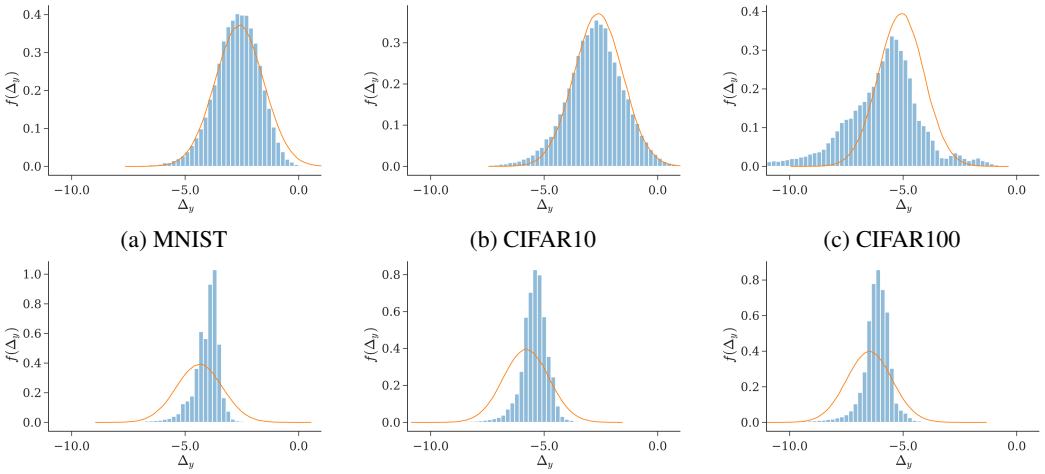

(a) MNIST (b) CIFAR10 (c) CIFAR100

(d) WebVision50 (e) WebVision200 (f) WebVision400

Figure 6: Comparisons between simulated and real Δ_y distributions at initialization. The simulations are based on the assumption that class scores follow normal distribution $s_i \sim \mathcal{N}(0, 1)$ at initialization and plotted as curves. Real distributions are extracted with randomly initialized models and plotted as histograms. The vertical axis denotes probability density $f(\Delta_y)$.

Settings	Clean 0.0	Symmetric 0.2	0.4	0.6	0.8	Asymmetric 0.1	0.2	0.3	0.4	Human 0.4
MAE shift	2.0	2.6	3.0	4.0	4.0	2.6	2.6	3.0	3.0	2.6
MAE scale	2.0	2.6	2.6	3.0	4.0	2.6	2.6	3.0	3.0	2.6
AGCE shift	4.0	4.0	4.0	5.0	5.0	4.0	4.0	4.0	4.0	4.0
AGCE scale	2.6	3.0	4.0	5.0	5.0	3.0	3.0	3.0	3.0	4.0

Table 10: Hyperparameter τ of $w^*(\Delta_y)$ and $w^+(\Delta_y)$ for different noise settings on CIFAR100. For reference, $\mathbb{E}[\Delta_y] = 5.097$ on CIFAR100 and $\mathbb{E}[\Delta_y] = 2.717$ on CIFAR10. Better performance can be achieved with a more thorough hyperparameter search.

Derivation of $\mathbb{E}(\Delta_y)$ at initialization in Eq. (9):

$$
\begin{aligned}
\mathbb{E}(\Delta_y) &= \mathbb{E}[s_y - \log \sum_{i \neq y} e^{s_i}] = \mu - \mathbb{E}[\log \sum_{i \neq y} e^{s_i}] \\
&\approx_1 \mu - \log \mathbb{E}[\sum_{i \neq y} e^{s_i}] + \frac{\mathbb{V}[\sum_{i \neq y} e^{s_i}]}{2\mathbb{E}[\sum_{i \neq y} e^{s_i}]^2} \\
&=_2 \mu - \log\{(k-1)\mathbb{E}[e^{s_y}]\} + \frac{(k-1)\mathbb{V}[e^{s_y}]}{2\{(k-1)\mathbb{E}[e^{s_y}]\}^2} \\
&=_3 \mu - \log[(k-1)e^{\mu+\sigma^2/2}] + \frac{(k-1)(e^{\sigma^2}-1)e^{2\mu+\sigma^2}}{2[(k-1)e^{\mu+\sigma^2/2}]^2} \\
&= -\log(k-1) - \sigma^2/2 + \frac{e^{\sigma^2}-1}{2(k-1)}
\end{aligned}
$$

where $\approx_1$ follows the approximation with Taylor expansion $\mathbb{E}[\log X] \approx \log \mathbb{E}[X] - \mathbb{V}[X]/(2\mathbb{E}[X]^2)$ (Teh et al., 2006), $=_2$ utilizes properties of sum of log-normal variables (Cobb et al., 2012), and $=_3$ substitutes $\mathbb{E}[e^{s_y}]$ and $\mathbb{V}[e^{s_y}]$ with expressions for log-normal distributions.

C.1.1 Addressing Underfitting from Marginal Initial Sample Weights

Hyperparamter τ for different settings The hyperparameter τ controlling the shape of modified sample-weighting functions $w^+(\Delta_y)$ and $w^*(\Delta_y)$ can affect the noise robustness. Thus we tune τ for the best performance under different noise types and noise rates, which are listed in Table 10. A larger noise rate η requires a larger τ to avoid overfitting noisy samples.

Loss	Clean $\eta = 0$	Symmetric Noise (Noise Rate η) $\eta = 0.2$	$\eta = 0.4$	$\eta = 0.6$	$\eta = 0.8$
CE‡	71.33 ± 0.43	56.51 ± 0.39	39.92 ± 0.10	21.39 ± 1.17	7.59 ± 0.20
GCE‡	63.09 ± 1.39	61.57 ± 1.06	56.11 ± 1.35	45.28 ± 0.61	17.42 ± 0.06
NCE‡	29.96 ± 0.73	25.27 ± 0.32	19.54 ± 0.52	13.51 ± 0.65	8.55 ± 0.37
NCE+AUL‡	68.96 ± 0.16	65.36 ± 0.20	59.25 ± 0.23	46.34 ± 0.21	23.03 ± 0.64
AGCE	49.27 ± 1.03	49.17 ± 2.15	47.76 ± 1.75	38.17 ± 1.43	16.03 ± 0.59
AGCE shift	69.39 ± 0.84	62.81 ± 0.42	48.21 ± 1.06	36.70 ± 2.89	14.49 ± 0.17
AGCE scale	70.57 ± 0.62	64.73 ± 0.98	56.69 ± 0.33	39.02 ± 1.20	14.64 ± 0.79
MAE	3.69 ± 0.59	2.92 ± 0.46	1.29 ± 0.50	2.27 ± 1.24	1.00 ± 0.00
MAE shift	69.02 ± 0.78	59.75 ± 0.84	44.60 ± 0.24	24.27 ± 0.26	8.08 ± 0.26
MAE scale	**70.97 ± 0.41**	**66.83 ± 0.84**	**60.57 ± 1.04**	**49.23 ± 1.22**	**24.44 ± 0.73**

Table 11: Addition results to Table 3 with more symmetric label noise rates on CIFAR100.

Loss	Clean $\eta = 0$	Asymmetric Noise (Noise Rate η) $\eta = 0.1$	$\eta = 0.2$	$\eta = 0.3$	$\eta = 0.4$
CE‡	71.33 ± 0.43	64.85 ± 0.37	58.11 ± 0.32	50.68 ± 0.55	40.17 ± 1.31
GCE‡	63.09 ± 1.39	63.01 ± 1.01	59.35 ± 1.10	53.83 ± 0.64	40.91 ± 0.57
NCE‡	29.96 ± 0.73	27.59 ± 0.54	25.75 ± 0.50	24.28 ± 0.80	20.64 ± 0.40
NCE+AUL‡	68.96 ± 0.16	66.62 ± 0.09	63.86 ± 0.18	50.38 ± 0.32	38.59 ± 0.48
AGCE	49.27 ± 1.03	47.53 ± 0.73	46.77 ± 2.37	39.82 ± 2.70	33.40 ± 1.57
AGCE shift	69.39 ± 0.84	63.03 ± 0.42	55.84 ± 0.78	49.05 ± 0.81	40.76 ± 0.74
AGCE scale	70.57 ± 0.62	67.13 ± 0.60	59.71 ± 0.10	48.23 ± 0.29	39.71 ± 0.17
MAE	3.69 ± 0.59	3.59 ± 0.56	3.19 ± 0.98	2.11 ± 1.93	2.53 ± 1.34
MAE shift	68.57 ± 0.54	63.44 ± 0.32	56.47 ± 0.48	48.79 ± 1.22	39.83 ± 0.18
MAE scale	**70.97 ± 0.41**	**69.50 ± 0.24**	**64.80 ± 0.49**	**59.04 ± 1.52**	**44.48 ± 1.05**

Table 12: Addition results to Table 3 with more asymmetric label noise rates on CIFAR100.

Additional results with $w^*(\Delta_y)$ and $w^+(\Delta_y)$. We report additional results under symmetric and asymmetric label noise with diverse noise rates η in Table 11 and Table 12, respectively. Performance of MAE and AGCE gets substantially improved with $w^*(\Delta_y)$ and $w^+(\Delta_y)$.

Visualization of $w^*(\Delta_y)$ and $w^+(\Delta_y)$. In Fig. 7 we visualize the shifted and scaled sample-weighting functions of MAE on CIFAR100. Although both achieve the same initial sample weights at $|\mathbb{E}[\Delta_y]|$ of CIFAR100, $w^+(\Delta_y)$ diminishes much faster as Δ_y increases, leading to insufficient learning of training samples, which can explain its inferior performance in Tables 3, 4, 11 and 12.

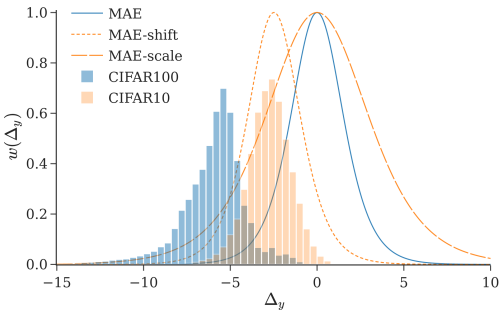

Figure 7: Shifted, scaled and the vanilla sample-weighting functions of MAE on CIFAR100. τ equals $|\mathbb{E}[\Delta_y]|$ on CIFAR10. We include the initial Δ_y distributions extracted with a randomly initialized model as reference.

	AUL	AGCE	GCE	SCE
a	2.0	3.0	/	/
q	2.0	4.0	0.4	0.95

Table 13: Hyperparameters of different loss functions for results in §4.2 and Appendix C.2. They are selected for broad coverage of shapes, scales and horizontal locations of sample-weighting functions instead of optimal performance on CIFAR10.

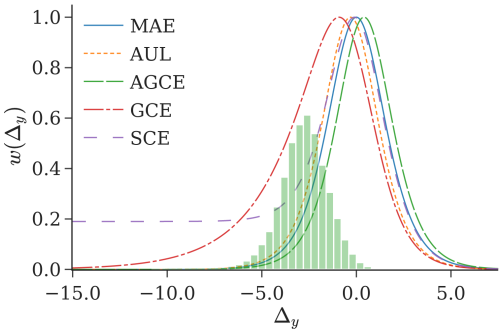

Figure 8: Plots of sample-weighting functions of loss functions used in Table 5 with hyperparameters in Table 8.

C.2 Noise Robustness of Loss Functions

Computation of $\bar{w}_{\text{clean}}$ and $\bar{w}_{\text{noise}}$ for snr in Table 5 The average weight for clean samples, adjusted by the learning rate at each step α_t, can be

$$\bar{w}_{\text{clean}} = \frac{\sum_{i,t} \alpha_t \cdot \mathbb{I}(\tilde{y}_{i,t} = y_{i,t}) w_{i,t}}{\sum_{i,t} \alpha_t \cdot \mathbb{I}(\tilde{y}_{i,t} = y_{i,t})}$$

where $w_{i,t}$ denotes the weight of i-th sample of the batch at step t, $\tilde{y}_{i,t}$ is the potentially corrupted noisy label and $y_{i,t}$ the uncorrupted label. Similarly, for noisy samples,

$$\bar{w}_{\text{noise}} = \frac{\sum_{i,t} \alpha_t \cdot \mathbb{I}(\tilde{y}_{i,t} \neq y_{i,t}) w_{i,t}}{\sum_{i,t} \alpha_t \cdot \mathbb{I}(\tilde{y}_{i,t} \neq y_{i,t})}$$

Hyperparameters We list the hyperparameters for different loss functions in Table 13 for results in §4.2 and Appendix C.2. In Fig. 8, we plot the sample-weighting functions of different loss functions.

Changes of Δ_y distributions with different label noise and loss functions Complementing Fig. 3, in Fig. 9 we plot how distributions of Δ_y change during training on CIFAR10 with additional types of label noise using hyperparameters in Table 13. They follow similar trends as in Fig. 3, thus supporting analysis in §4.2. As MAE is not robust against asymmetric label noise with high η (Ghosh et al., 2017), it results in inferior performance. We also include results with additional loss functions in Fig. 10. Since optimal hyperparameters will result in similar sample-weighting functions, we choose hyperparameters for broad coverage of $w(\Delta_y)$ to better understand how they affect robustness.

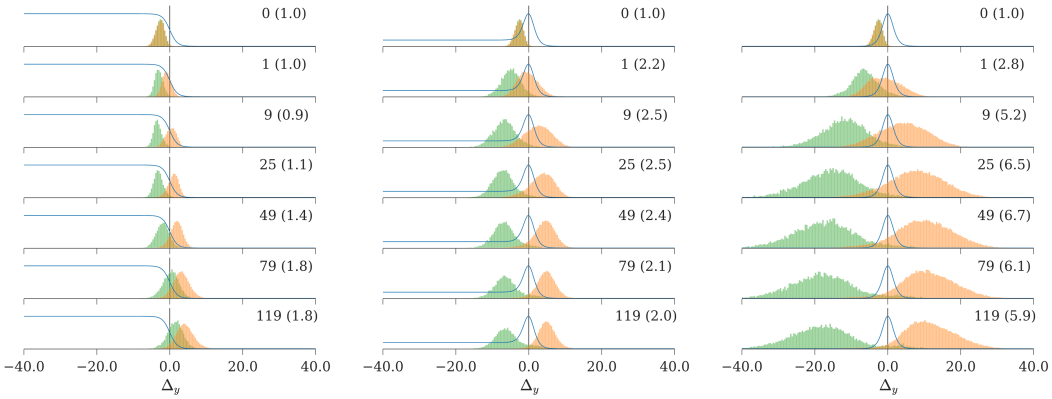

(a) CE, Sym., 0.2: 74.49 (b) SCE, Sym., 0.2: 85.31 (c) MAE, Sym., 0.2: 86.71

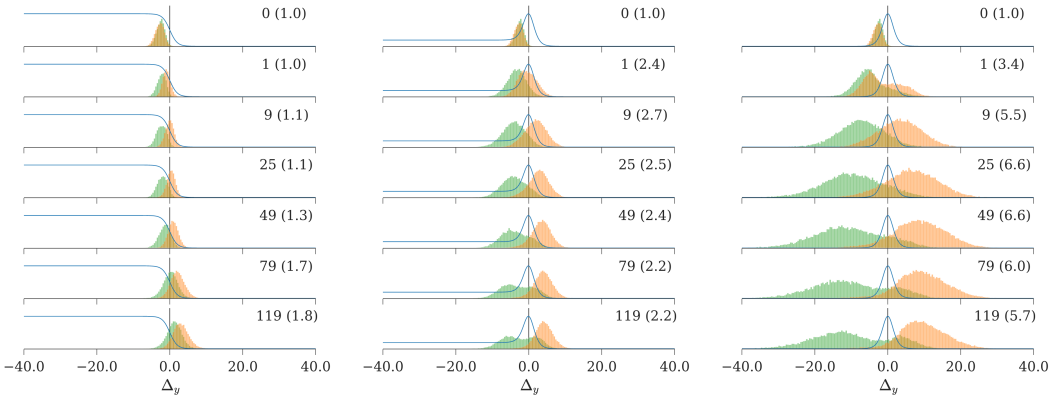

(d) CE, Human, 0.4: 61.12 (e) SCE, Human, 0.4: 72.56 (f) MAE, Human, 0.4: 78.99

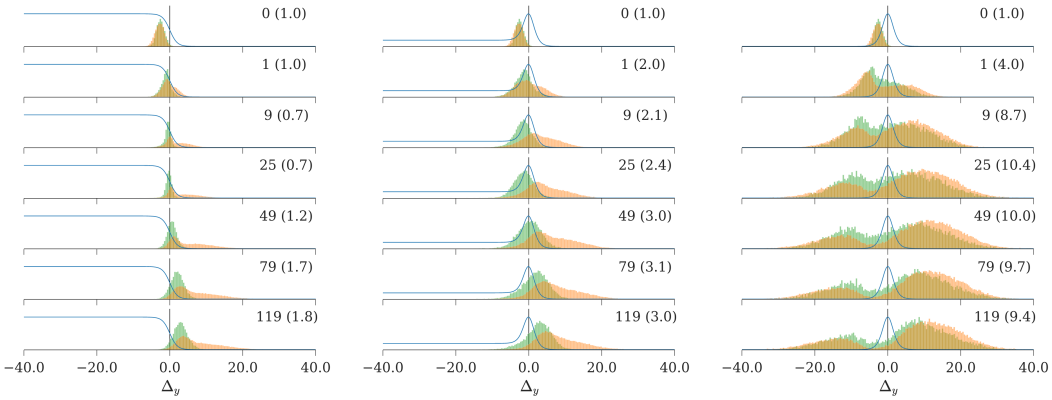

(g) CE, Asym., 0.4: 73.75 (h) SCE, Asym., 0.4: 72.44 (i) MAE, Asym., 0.4: 61.11

Figure 9: Additional results to Fig. 3 with different label noise: (a-c) symmetric label noise with $\eta = 0.2$; (d-f) human label noise with $\eta = 0.4$; (g-i) asymmetric label noise with $\eta = 0.4$. Noisy samples are colored green (on the left) and clean samples are orange (on the right). Test accuracies are included in the caption for reference.

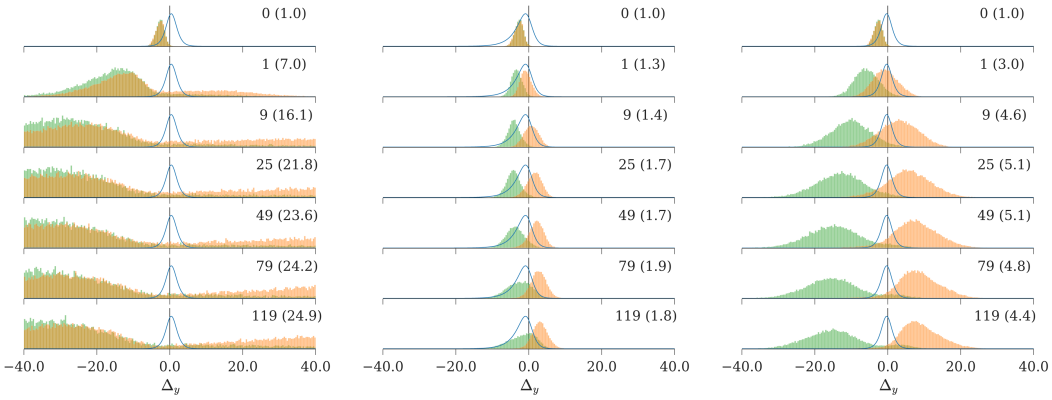

(a) AGCE, Sym., 0.4: 44.52

(b) GCE, Sym., 0.4: 66.60

(c) AUL, Sym., 0.4: 84.12

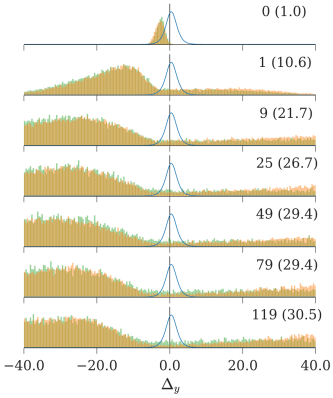

(d) AGCE, Human, 0.4: 35.73

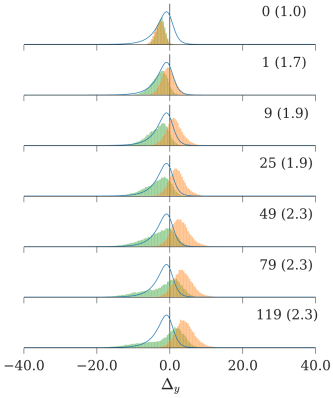

(e) GCE, Human, 0.4: 68.22

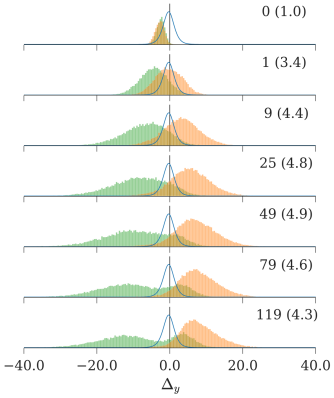

(f) AUL, Human, 0.4: 77.22

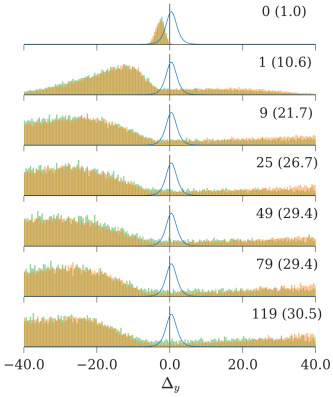

(g) AGCE, Asym., 0.4: 46.75

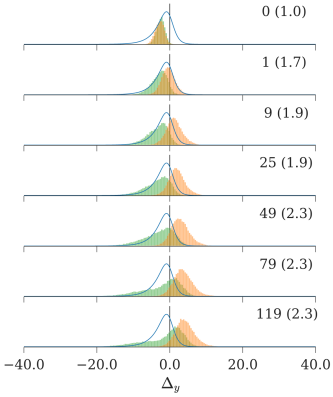

(h) GCE, Asym., 0.4: 73.23

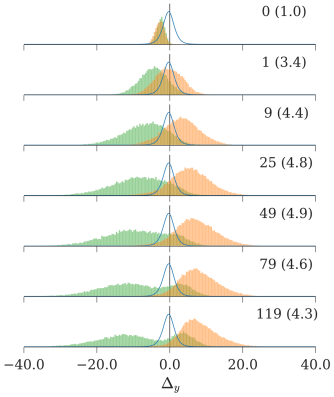

(i) AUL, Asym., 0.4: 67.72

Figure 10: Additional results to Fig. 3 with more robust loss functions under different label noise: (a-c) symmetric label noise with $\eta = 0.4$; (d-f) human label noise with $\eta = 0.4$; (g-i) asymmetric label noise with $\eta = 0.4$. Test accuracies are included in the caption for reference. Noisy samples are colored green (on the left) and clean samples are orange (on the right). Hyperparameters of these loss functions are selected for broad coverage rather than optimal performance.